Predicting the Stability of Fullerene Allotropes Throughout the Periodic Table

Qing Zhao[1, 2], Stanley S. H. Ng[1], and Heather J. Kulik[1, *]

[1]*Department of Chemical Engineering, Massachusetts Institute of Technology, Cambridge, MA 02139*

[2]*Department of Mechanical Engineering, Massachusetts Institute of Technology, Cambridge, MA 02139*

We present a systematic study of the role of elemental identity in determining electronic, energetic, and geometric properties of representative $A_{28}B_{28}$, $A_{30}B_{30}$, and $A_{36}B_{36}$ III-V (A=B, Al, Ga, or In and B=N, P, or As) and II-VI (A=Zn or Cd and B=S or Se) fullerene allotropes. A simple descriptor comprised of electronegativity differences and covalent radii captures the relative fullerene stability with respect to a nanoparticle reference, and we demonstrate transferability to group IV A_{72} (A=C, Si, or Ge) fullerenes. We identify the source of relative stability of the four- and six-membered-ring-containing $A_{36}B_{36}$ and $A_{28}B_{28}$ fullerene allotropes to the less stable, five-membered-ring containing $A_{30}B_{30}$ allotrope. Relative energies of hydrogen-passivated single ring models explain why the even-membered ring structures are typically more stable than the $A_{30}B_{30}$ fullerene, despite analogies to the well-known C_{60} allotrope. The ring strain penalty in the four-membered ring is comparable to or smaller than the nonpolar bond penalty in five-membered rings for some materials, and, more importantly, five-membered rings are more numerous in $A_{30}B_{30}$ than four-membered rings in $A_{36}B_{36}$ or $A_{28}B_{28}$ allotropes. Overall, we demonstrate a path forward for predicting the relative stability of fullerene allotropes and isomers of arbitrary shape, size, and elemental composition.

1. Introduction

Thirty years after the discovery of Buckminsterfullerene (C_{60}) through vaporization of graphite by laser irradiation[1], the excellent properties and potential applications of this unusual carbon allotrope continue to drive considerable scientific inquiry[2]. Since their initial discovery, C_{60} fullerenes have found broad technological relevance in polymer-fullerene solar cells[3-6], drug delivery[7-8], and proposed hydrogen storage devices[9]. The unusual shape and properties of C_{60} have motivated study of its formation mechanism both theoretically[10] and experimentally[11]. Soon after the discovery of the carbon-based fullerene, isoelectronic boron nitride fullerenes were synthesized by electron beam irradiation[12] and later with more success through the arc-melting method in a wide size range (B_nN_n, n=12[13], 24[14-15], 28[15], 36[15-17], and 48[15]). These structures differ from C_{60} in that they are proposed to only have even-membered rings with polar B-N bonds, although transition metal dopants[16-17] have also been observed to be present due to synthesis conditions. We note that elemental boron, in particular, is well known to produce unusual chemical bonding and allotropes[18-19]. Recently, hollow nanocage structures have been made from other elements, including an all boron fullerene[20] and multilayered inorganic MoS_2[21-24] and $MoSe_2$[21] fullerene-like structures.

First-principles simulation can provide valuable insight into the relationship between the unusual geometric structure and associated electronic properties for both fullerenes that have been experimentally isolated and those that may yet still be synthesized. Of all of the binary fullerenes, boron nitride structures have been the primary focus of numerous computational semiempirical[25] and density functional theory (DFT)[26-33] studies, primarily at sizes commensurate with experimentally characterized BN fullerenes[25-27, 29-32], especially $B_{36}N_{36}$[26-27, 29-31] allotropes, or slightly larger structures[28, 33]. Simulations have estimated the 72-atom

fullerene to be most stable when 6 four-membered and 32 six-membered rings are present[26], although there has been some exploration[28-29] of line defects, octagons, decagons and dodecagons or with transition metal dopants[30] and hydrogenated structures[33]. Beyond boron nitride, there have been fewer studies of binary compounds comprised of other elements, and typically the focus has been on III-V and II-VI binary A_nB_n fullerenes with light elements[34-46] (A=boron, aluminum, zinc; B=nitrogen, phosphorus, oxygen, sulfur) and small size[34-35, 38-47] (n=12). There are a few exceptions in the literature with heavier elements[45, 47-49] (A=gallium, cadmium; B=arsenic) and larger sizes[36-37, 48-49], and binary IV-IV $Si_{12}C_{12}$[35] and homogeneous boron fullerenes[50-51] have also been considered. One notable exception is a study by Beheshtian and coworkers[34] who focused on a broader view of the role that element substitution plays in $A_{12}B_{12}$ (A=boron, aluminum; B=nitrogen, phosphorus) fullerene properties. In addition to fundamental property studies, some investigations have focused on the potential of binary or ternary III-V[52-53] or II-VI[54-56] fullerenes in nanotechnology as gas sensors, for drug delivery[57], or as hydrogen storage materials[58-62].

Despite numerous theoretical studies of structural, energetic, and electronic properties of III-V and II-VI binary fullerenes, a thorough analysis of fullerenes throughout the periodic table has not thus far been carried out in order to identify underlying chemical trends in stable fullerene allotrope candidates. A better understanding of the element-specific rules that govern fullerene allotrope stability will help accelerate identification of potentially synthetically accessible candidates with novel materials properties. Here, we provide a comprehensive study of the relative stability and properties of A_nB_n (n=28, 30, 36) fullerenes for 12 III-V materials (A=B,Al,Ga, or In and B=N, P, or As), 4 II-VI materials (A=Zn or Cd and B=S or Se) with some

comparison to unary IV C, Si, and Ge structures. In this study, we unearth simple, global descriptors and structural models capable of predicting fullerene stabilities.

The outline of the paper is as follows. In Section 2, we present the Computational Details of our study. Section 3 contains the Results and Discussion of the energetic and electronic properties of stoichiometric III-V and II-VI $A_{36}B_{36}$ fullerenes along with comparisons and evaluations of properties to $A_{28}B_{28}$ and $A_{30}B_{30}$ fullerenes. We provide our Conclusions in Section 4.

2. Computational Details

First-principles simulations. Calculations were carried out with the graphical-processing unit (GPU)-accelerated quantum chemistry package, TeraChem[63-64]. Geometry optimizations[65] and band gap calculations were performed using DFT with the long-range corrected, hybrid ωPBEh[66] exchange-correlation functional (ω=0.2) and the composite LACVP* basis set. The LACVP* basis set corresponds to an LANL2DZ effective core potential basis for the Zn, Cd, Ga, In, As, and Se atoms and 6-31G* basis for the B, Al, N, P, and S atoms.

Structures. We used the $B_{36}N_{36}$ ($B_{28}N_{28}$) fullerene geometry obtained with the CRYSTAL14[67] package as a starting point to generate all other $A_{36}B_{36}$ ($A_{28}B_{28}$) fullerenes. We converted the $B_{36}N_{36}$ ($B_{28}N_{28}$) Cartesian coordinates to internal coordinates in the Gaussian z-matrix format, replaced boron or nitrogen atoms by A or B atoms, respectively, and initially rescaled interatomic distances in the z-matrix based on experimental A-B bond distances in AB crystal structures[68]. The optimal bond distances for the starting point of geometry optimizations of $A_{36}B_{36}$ fullerenes were obtained by scanning distances in 0.05 Å increments within ± 0.5 □ of the experimental bond distances. Initial $A_{30}B_{30}$ fullerene configurations were built following the

$A_{36}B_{36}/A_{28}B_{28}$ procedure but instead starting from a C_{60} fullerene geometry obtained from the Fullerene Library[69]. In order to investigate the stability of $A_{36}B_{36}$ fullerenes, we also built unpassivated $A_{36}B_{36}$ spherical nanoparticles (NPs). We obtained experimental parameters of AB crystals from the Crystallography Open Database[68], built supercells of the AB bulk in Avogadro[70], and removed unneeded atoms from the super cells to form spherical NPs. In order to understand stability difference between $A_{30}B_{30}$ and $A_{36}B_{36}$ fullerenes, initial passivated four-, five-, six-membered rings were built using experimental bond distances[68] with Avogadro[70].

Analysis. Coordination numbers (CNs) of individual atoms in fullerenes and NPs are assigned based on rescaled covalent radii of A and B atoms. The cutoff for an A-B bond was assigned as:

$$d_{\text{cut}}(\text{A-B}) = 1.25(r_{\text{cov}}^{\text{A}} + r_{\text{cov}}^{\text{B}}), \quad (1)$$

where $r_{\text{cov}}^{\text{A}}$ is covalent radius of A atom and $r_{\text{cov}}^{\text{B}}$ is covalent radius of B atom. The tabulated distance cutoffs for A-B bonds in all studied materials are summarized in Supporting Information Table S1. Partial charges of atoms and bonding analysis were obtained from the TeraChem interface with the Natural Bond Orbital (NBO), version 6.0 package[71]. NBO calculates the natural atomic orbitals (NAOs) for each atom by computing the orthogonal eigenorbitals of the atomic blocks in the density matrix, and the NBO partial charge on an atom is obtained as the difference between the atomic number and the total population for the NAO on the atom. The Pauling electronegativity difference[72] (see Supporting Information Table S2), which is defined as the dissociation energy difference between A-B bonds and the average of A-A and B-B bonds, was used to analyze the fullerene stability and bonding properties. The projected density of states (PDOS) was computed for fullerenes by extracting the square of

coefficients of atom-centered basis functions of each angular momentum type and applying Gaussian broadening (σ=0.01 Ha) using an in-house Python script.

3. Results and Discussion

3a. Energetics of $A_{36}B_{36}$ Fullerenes

We investigated the energetic properties of $A_{36}B_{36}$ fullerenes from stoichiometric combinations of i) III-V group elements: A = boron, aluminum, gallium, or indium with B = nitrogen, phosphorus, or arsenic and ii) II-VI group elements: A = zinc or cadmium with B = sulfur or selenium. The $A_{36}B_{36}$ structure consists of four- and six-membered rings that contain only A-B bonds and no A-A or B-B bonds, unlike a five-membered-ring-containing binary $A_{30}B_{30}$ model of Buckminsterfullerene (Figure 1). The 6 four-membered rings reside on the vertices of the $A_{36}B_{36}$ octahedral structure that also contains 32 six-membered rings.

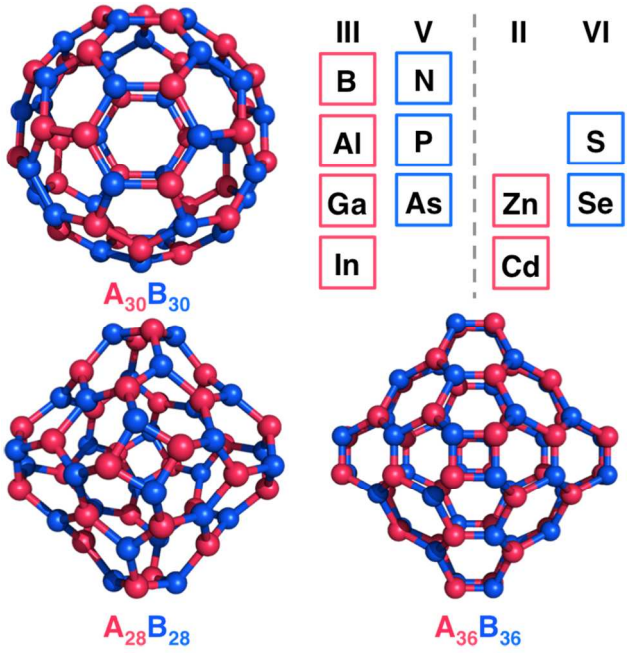

Figure 1. Representative ball-and-stick models of $A_{30}B_{30}$ (top left), $A_{28}B_{28}$ (bottom left), and

$A_{36}B_{36}$ (bottom right) fullerenes with A atoms shown in red and B atoms in blue. The A and B element choices are shown at top right: A atoms from group III (in red boxes) with B atoms from group V (in blue boxes) or A atoms from group II (in red boxes) with B atoms from group VI (in blue boxes).

Geometry optimization of initial $A_{36}B_{36}$ fullerene structures (see Computational Details) preserves coordination and qualitative structure with no bond rearrangement. However, the alternating short and long bond lengths in the initial structures become more comparable after geometry optimization (see Supporting Information Table S3). This unchanged coordination indicates that the fullerenes are stable local minima, but comparison to other allotropes is needed to infer global stability. We used nanoparticles (NPs) cut from bulk crystal structures, as is common practice in semiconductor NP studies[73-74], with the same number of atoms as a fullerene in order to provide a candidate low energy reference (see Supporting Information Figure S1). For consistency, we geometry optimized these unpassivated NP structures. The average initial CN for the spherical NPs is 3, the same as in a fullerene. NP geometry optimizations result in surface rearrangement, increasing the average CN of each compound to between 3.1 and 3.7 (see Supporting Information Table S4). Although we expect the NPs to be more stable than the fullerene structures due to higher average CNs in the optimized NPs, there is a trade-off with some surface atoms (CN < 3) in the reconstructed NPs.

In order to determine the relative stability of $A_{36}B_{36}$ fullerenes, we define a relative energy per pair of A, B atoms in optimized fullerenes (E(FL)) with respect to those in the optimized NP (E(NP):

$$E_{\text{per pair}} = \frac{E(\text{FL})}{36} - \frac{E(\text{NP})}{36} \quad . \tag{2}$$

We have previously used a similar metric in the analysis of amorphous InP cluster stability[75]. Interestingly, the fullerenes are more stable than NPs (i.e., the energy per pair is negative) for almost all materials studied (Figure 2). These observations suggest, for instance, that the four-membered rings present in the fullerenes do not induce significant strain, which we will consider in more detail shortly when we compare to other fullerene allotropes that lack four-membered rings. The most stable fullerene (-28 kcal/mol per pair) is $B_{36}N_{36}$, which has already been successfully synthesized experimentally[15-17]. In addition to this well-studied compound, $Al_{36}N_{36}$, $Ga_{36}N_{36}$, $In_{36}N_{36}$, and $B_{36}P_{36}$ fullerenes are all more stable than the optimized NPs by at least 5 kcal/mol per pair. Comparing all element choices, fullerene relative stability decreases when an anion or cation is held fixed and the other species (cation or anion) is substituted with a heavier element. For all 16 compounds considered, we identify only the II-VI $Cd_{36}Se_{36}$ fullerene ($E_{\text{per pair}}$ = 4 kcal/mol) as an exception where the NP is more stable. We note, however, that II-VI fullerenes are generally less stable than III-V fullerenes. This trend may be in part due to larger charge separation in the II-VI materials than that of III-V materials. Overall, our observations suggest the following candidates for experimentally stable fullerenes: $Al_{36}N_{36}$, $Ga_{36}N_{36}$, $In_{36}N_{36}$, and $B_{36}P_{36}$ in addition to the previously-characterized $B_{36}N_{36}$.

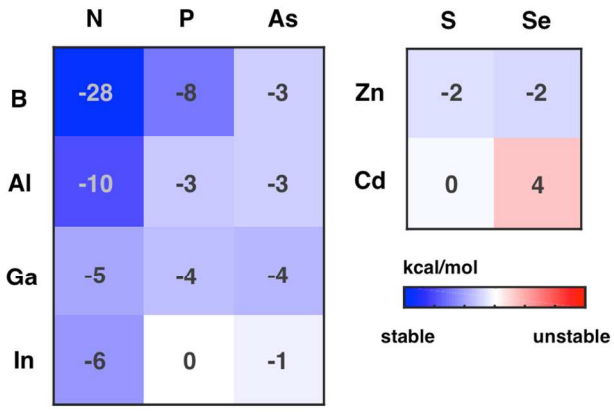

Figure 2. Relative energy per pair of AB atoms in kcal/mol of geometry-optimized $A_{36}B_{36}$ fullerenes and nanoparticles for different III-V group (left) and II-VI group (right) compounds. The materials for which the fullerenes are most stable are indicated in blue, and those for which the nanoparticles are most stable are indicated in red. The color scale is centered at 0 kcal/mol and saturated values correspond to +/- 15 kcal/mol, as indicated by the inset color bar.

We investigated several candidate descriptors to unearth explanations for these observed trends in $A_{36}B_{36}$ fullerene stability. These descriptors included: i) the sum of A and B atoms' atomic numbers, ii) the sum of covalent radii, iii) A-B bond lengths of geometry optimized $A_{36}B_{36}$ fullerenes, and iv) electronegativity differences between A and B atoms. We found that no single descriptor correlated sufficiently strongly to stability trends (see Supporting Information Figure S2). Instead, we identified a linear combination of properties that describes relative stability trends (Figure 3). Our search for a best-fit relationship between relative stability and descriptors reveals a simple functional form (R^2=0.80):

$$E_{\text{per pair}} = 30.04\left[0.31\left|\Delta\chi_{\text{B-A}} - 0.75\right| + 0.69\left(r_{\text{cov}}^{\text{A}} + r_{\text{cov}}^{\text{B}}\right)\right] - 53.59 , \quad (3)$$

where $E_{\text{per pair}}$ is the relative energy per pair of A and B atoms in kcal/mol, $\Delta\chi_{\text{B-A}}$ is the unitless Pauling electronegativity difference between B and A atoms, $r_{\text{cov}}^{\text{A}}$ and $r_{\text{cov}}^{\text{B}}$ are covalent radii of A and B atoms in □. This expression suggests that stability is determined roughly 30% by the electronegativity difference and 70% by the effective size of the substituent elements, which generally increases as we move down the periodic table. The centering of electronegativity differences around -0.75 was based on an analysis of trends in stability versus electronegativity alone (see Supporting Information Figure S2).

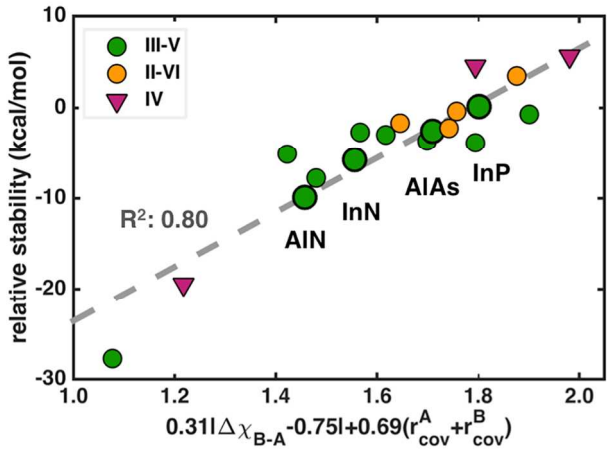

Figure 3. Relationship of the relative energy per pair of AB atoms in kcal/mol of $A_{36}B_{36}$ fullerenes referenced against spherical nanoparticles from III-V (green circles), II-VI (orange circles), and IV (magenta triangles) materials with a linear combination of electronegativity difference of B and A atoms ($\Delta\chi_{\text{B-A}}$) and sum of covalent radius of A ($r_{\text{cov}}^{\text{A}}$) and B ($r_{\text{cov}}^{\text{B}}$) atoms. A best-fit line (gray dashed), which was fit only to III-V and II-VI data, is shown. Selected compounds are labeled and highlighted with bolder symbols.

In order to test the transferability of the observed trend, we investigated whether group IV single-element A_{72} fullerenes (A=C, Si, Ge) stability would follow the same trend as the

binary fullerenes. We note here the electronegativity difference is zero ($\Delta\chi_{\text{A-A}} = 0$) and the covalent radii are identical ($r_{\text{cov}}^{\text{B}} = r_{\text{cov}}^{\text{A}}$) (see Supporting Information Method S1 for details of computing the relative stability of A_{72} fullerenes). Our combined descriptor of electronegativity and covalent radius predicts not only the relative stability of $A_{36}B_{36}$ fullerenes but also that of the homogenous A_{72} fullerenes (Figure 3).

3b. Electronic Properties of $A_{36}B_{36}$ Fullerenes

We then studied the role that elemental composition plays in determining electronic properties of the $A_{36}B_{36}$ fullerenes. Band gaps may be obtained from total energy differences of cationic, anionic, and neutral species, which is commonly called the Δ-SCF method[76-77], or approximated as the Kohn-Sham gap obtained from the difference in highest-occupied molecular orbital (HOMO) and lowest-unoccupied molecular orbital (LUMO) energies. Generally, the HOMO-LUMO Kohn-Sham gap is known to be quite close to the fundamental gap for generalized Kohn-Sham methods such as range-corrected hybrids[78-79]. We verified the validity of this observation for C_{60} fullerenes by comparing ωPBEh[66] HOMO-LUMO (6.0 eV) and Δ-SCF (5.9 eV) gaps with each other and to the experimental value (4.9 eV[80]). Range-separation parameter (ω□□ tuning to match the negative of the HOMO eigenvalue ($-\varepsilon_{\text{HOMO}}$) to the ionization potential (IP) has been demonstrated[79] as a strategy to obtaining improved optical properties of materials. Notably, our use of the default ω parameter (0.2) yields a difference of only 0.06 eV between the IP and $-\varepsilon_{\text{HOMO}}$, indicating this value is suitable for the materials studied. Although ωPBEh overestimates the gap, the HOMO-LUMO gap and fundamental gap are quite close, and the overall error is reduced with respect to global hybrids, such as B3LYP[81-

[82] (see Supporting Information Figure S3). Therefore we focus on trends in the gaps predicted with ωPBEh, anticipating that calculated gaps are likely slight overestimates.

Comparison of geometry-optimized III-V and II-VI $A_{36}B_{36}$ fullerenes reveals a significant variation from HOMO-LUMO gaps as small as 5.3 eV for heavy elements to as large as 10.8 eV for the lightest element pairings (Figure 4). Some $A_{36}B_{36}$ (B=nitrogen) fullerenes have been previously studied with the PBE functional[83], yielding predicted band gaps of 5.1 eV (A=boron), 2.7 eV (A=aluminum), 2.2 eV (A=gallium) and 0.7 eV (A=indium). The PBE functional is known to underestimate band gaps[83], but focusing on band gap trends indicates a comparable 5 eV difference from the lightest to heaviest fullerenes. This band gap shift is also consistent with the shift observed experimentally for AB crystal structures (from 6.2 eV to 0.42 eV[80, 84-85]) with increasingly heavy cation or anion substitutions (see Supporting Information Table S5). Confinement effects in the 0D fullerene structure as well as the slight overestimate of band gaps previously noted for ωPBEh explain this difference with respect to the bulk crystal structure. In contrast with overall trends, we note several exceptions to the band gap reduction with increasing mass. Interestingly, these exceptions in our DFT calculations (AlP, GaP > BP and AlAs > BAs) follow trends observed in experimental bulk crystal band gaps.

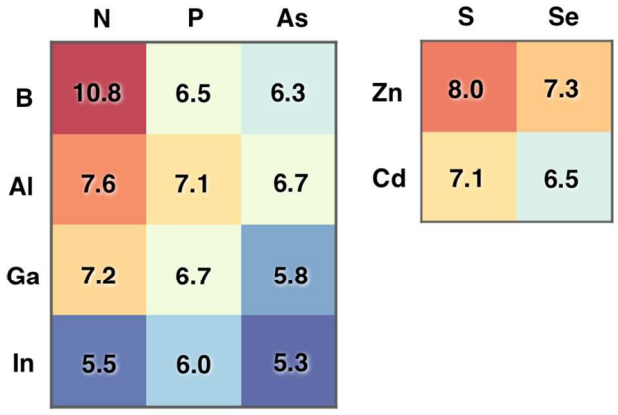

Figure 4. HOMO-LUMO gaps (in eV) of geometry-optimized $A_{36}B_{36}$ fullerenes from III-V (left) and II-VI (right) materials obtained with ωPBEh/LACVP*. HOMO-LUMO gaps are color-coded by magnitude from largest (red) to smallest (blue).

In order to compare substitution of A and B elements, we calculated the average change in band gap by keeping the cation (anion) element the same and moving to a heavier anion (cation) element as 1.0 eV and 1.1 eV, respectively, indicating comparable effects in band gaps of substitution of A and B elements. A direct comparison of the dependence of individual HOMO and LUMO eigenvalues with element substitution (see Supporting Information Figure S4) reveals separate effects of the cation and anion, however. When the cation element is kept the same for III-V or II-VI materials, LUMO eigenvalues show a relatively wider dependence on substitution of different anion elements compared with HOMO eigenvalues, indicating anion elements tend to change the LUMO more. Comparable ranges of HOMO and LUMO shifts are observed by keeping anion the same for III-V materials or II-VI materials, indicating cation elements change HOMO and LUMO equally.

In order to compare how substitutions of cationic and anionic elements change electronic structure, we present the total and orbital projected density of states (PDOS) of A=boron, gallium, or B=nitrogen, phosphorus in $A_{36}B_{36}$ fullerenes (Figure 5). Moving down the periodic table shifts the peaks near the Fermi level in both the conduction band (CB) and valence band (VB), with the strongest effect observed from first-row to second-row nitrogen to phosphorus or boron to aluminum elements. In all cases, the VB is predominantly derived from the anion atom *p* orbitals, varying from 40% to 71% for the compounds considered (see Supporting Information

Table S6), with lighter anion fullerenes exhibiting the largest *p* orbital contributions. Notably, cation effects are not monotonic, and gallium-containing fullerenes possess the most anion *p* orbital contributions. Owing to charge transfer effects, the CB is in turn dominated by cation *p* orbitals with the lightest nitrogen-containing fullerenes having the largest contribution.

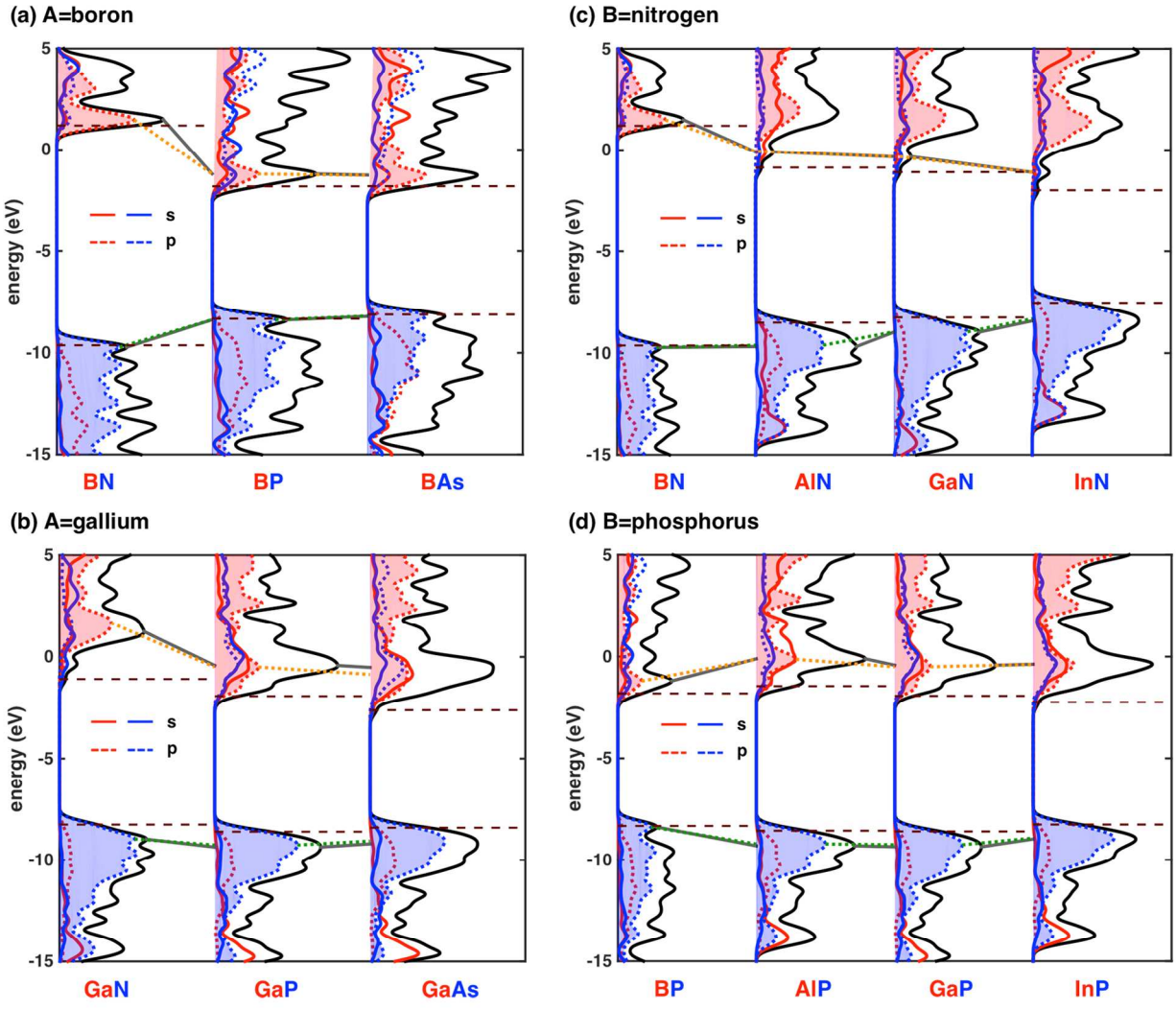

Figure 5. Total density of states (DOS) (black line) and orbital projected density of states (PDOS) of A atom s orbital (red solid line), A atom *p* orbital (red dashed line), B atom *s* orbital (blue solid line) and B atom *p* orbital (blue dashed line) for (a) A=boron, (b) A=gallium, (c) B=nitrogen, and (d) B=phosphorus fullerenes. The dominant orbitals in the VB and CB are

indicated with light blue and light red shaded regions. The shifts of DOS peaks (gray lines) and dominant orbitals peaks in PDOS of both the CB (orange dashed lines) and VB (green dashed lines) are highlighted between each material. The brown dashed lines indicate the positions of the HOMO and LUMO.

Specific trends depend strongly on the materials compared, e.g. from BN to BP the *p* orbital peaks in both the VB and CB shift toward the Fermi level. From GaN to GaP, on the other hand, the peak in the VB shifts away from the Fermi level and the CB peak shifts toward the Fermi level. From BN to AlN, the peak in the VB remains the same position and the CB peak shifts toward the Fermi level. From BP to AlP, both peaks in VB and CB shift away from the Fermi level. In contrast, when changing from second- to third-row phosphorus to arsenic anions or from aluminum to indium cations, the peaks in both the CB and VB keep similar positions (A=aluminum or indium and B=arsenic behave comparably to A=boron or gallium and B=phosphorus, as shown in Supporting Information Figure S5). The main exception to this latter trend is when comparing heavier cation substitution in B=nitrogen fullerenes, which leads to a gradual shift in *p* orbital peaks toward the Fermi level. The II-VI fullerenes behave comparably to the III-V materials but show less overall difference with element substitution (see Supporting Information Figure S5).

We can further explain trends in the PDOS by comparing NBO partial charges in different materials. The partial charge analysis reveals that both A and B atoms become more neutral with increasingly heavy anion atoms (see Supporting Information Figure S6), which explains the decreasing contributions of anion *p* orbitals in the VB. In contrast, the extent of

charge transfer is comparable for second- to fourth-row cation atoms, which is consistent with the comparable contributions of anion *p* orbitals in the VB with heavier cation atoms. Our definition of A (group III/group II) as the cation and B (group V/group VI) as the anion atoms holds except for the $B_{36}P_{36}$ and $B_{36}As_{36}$ fullerenes (Table 1), where the partial charges change sign. Notably, similar behavior has been observed in the computational study of other low-dimensional semiconducting materials[86]. Both the standard and reversed charges can be explained in terms of the electronegativity of the substituent atoms. The group V (group VI) elements generally have much higher electronegativities than group III (group II) elements, but the electronegativity of boron (2.04) is comparable to that of phosphorus (2.19) and arsenic (2.18). Indeed, charge transfer observed in these materials correlates well to electronegativity differences, even upon inclusion of the boron-containing fullerenes (see Supporting Information Figure S7).

Table 1. The net charge transfer from A to B atoms ($q_{A\text{-}B}$), the Pauling electronegativity difference between B and A atoms ($\Delta\chi_{B\text{-}A}$), and the extent of bonding character the A atom contributes in A-B bonds given by NBO analysis ($Bond_A$, in %) in $A_{36}B_{36}$ fullerenes.

System	$q_{A\text{-}B}$	$\Delta\chi_{B\text{-}A}$	$Bond_A$
BN	1.17	1.00	23
BP	-0.34	0.15	48
BAs	-0.56	0.14	51
AlN	1.90	1.43	11
AlP	1.18	0.58	23
AlAs	0.92	0.57	27
GaN	1.82	1.23	12
GaP	1.07	0.38	26
GaAs	0.79	0.37	30
InN	1.78	1.26	12

InP	1.29	0.41	22
InAs	1.01	0.40	27
ZnS	1.49	0.93	10
ZnSe	1.37	0.9	13
CdS	1.49	0.89	10
CdSe	1.36	0.86	13

We next determined the extent of covalent or ionic character in $A_{36}B_{36}$ fullerene A-B bonds with NBO analysis. Here, we use the extent of bonding character the A atom contributes as a proxy for the covalent character of a bond (Table 1). Charge transfer and ionic character is strongest for first-row-anion fullerenes, and the A-B bonds become increasingly covalent with heavier anion atoms. Conversely, the lightest cation A=boron fullerenes have the most covalent bonds, and the other III-group elements all exhibit more ionic bonding. The II-VI fullerenes extend this trend with even more ionic bonding. We can explain the relative covalency or ionicity by invoking each element's electronegativity. Our analysis of the relationship between percent of bonding orbital contribution from the A atoms in localized NBO orbitals ($Bond_A$, in %) and the unitless Pauling electronegativity differences between A and B atoms ($\Delta\chi_{B\text{-}A}$) reveals a log-log relation (R^2=0.81):

$$\log(Bond_A) = -0.69\log(\Delta\chi_{B\text{-}A}) + 1.13 \quad (4)$$

in the $A_{36}B_{36}$ fullerenes (Figure 6). Among all materials studied, there are three A-B fullerene bonds that are outliers for this relation: B-N bonds in $B_{36}N_{36}$ fullerenes are more covalent than expected, whereas Zn-S and Cd-S bonds in $Zn_{36}S_{36}$, and $Cd_{36}S_{36}$ fullerenes are more ionic than electronegativity differences alone would predict.

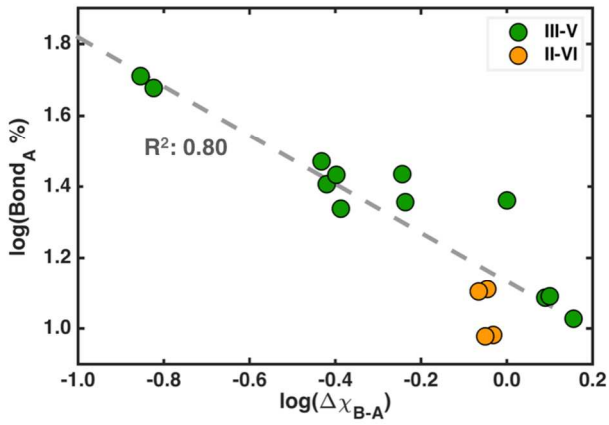

Figure 6. The extent of bonding character the A atom contributes in A-B bonds ($Bond_A$) of $A_{36}B_{36}$ fullerenes given by NBO analysis as a function of the unitless Pauling electronegativity difference between B and A atoms ($\Delta\chi_{B\text{-}A}$) in a log scale for III-V materials (green circles) and II-VI materials (orange circles). A linear best-fit line (gray dashed) is also shown.

3c. Comparisons of $A_{28}B_{28}$, $A_{30}B_{30}$ and $A_{36}B_{36}$ Fullerenes

Thus far, we have studied the energetic and electronic properties of $A_{36}B_{36}$ fullerenes and identified materials that are good candidates to form experimentally stable $A_{36}B_{36}$ fullerenes. A key question that remains is the extent to which $A_{36}B_{36}$ fullerenes may be more stable than the equivalent $A_{30}B_{30}$ Buckminsterfullerene-like allotropes. For $A_{36}B_{36}$ fullerenes, the presence of four-membered rings absent from the Buckminsterfullerenes may introduce strain. On the other hand, the covalent, nonpolar bonds present in the five-membered rings of $A_{30}B_{30}$ fullerenes but absent in $A_{36}B_{36}$ structures may be energetically unfavorable. Therefore, we surveyed energetic properties of the previously studied combinations of III-V and II-VI elements for $A_{30}B_{30}$ models, which have 20 six-membered rings and 12 five-membered rings with 6 nonpolar, A-A bonds and

6 nonpolar, B-B bonds (Figure 1). In addition, we investigated a smaller fullerene model, $A_{28}B_{28}$, which has been experimentally[15] and theoretically[25, 29] characterized for boron nitride, that contains 6 four-membered rings and 24 six-membered rings (Figure 1).

Geometry optimizations of both $A_{28}B_{28}$ and $A_{30}B_{30}$ fullerene structures preserve the coordination with no bond rearrangement. However, the alternating short and long bond lengths in the initial $A_{28}B_{28}$ structures become more comparable (see Supporting Information Table S7). In the $A_{30}B_{30}$ structures, the bond lengths become more disparate, corresponding to the distinct A-B, A-A, and B-B bonds (see Supporting Information Table S8). The lack of change in coordination indicates both $A_{28}B_{28}$ and $A_{30}B_{30}$ fullerenes are stable local minima. In order to compare the stability of these new fullerene structures with that of the $A_{36}B_{36}$ structures, we define a relative energy per pair of A, B atoms in the optimized $A_{28}B_{28}$ fullerene ($E(A_{28}B_{28})$) and $A_{30}B_{30}$ fullerene ($E(A_{30}B_{30})$) with respect to those in the optimized $A_{36}B_{36}$ fullerene ($E(A_{36}B_{36})$):

$$E_{\text{per pair}}(A_{28}B_{28}) = \frac{E(A_{28}B_{28})}{28} - \frac{E(A_{36}B_{36})}{36} \text{, and} \quad (5)$$

$$E_{\text{per pair}}(A_{30}B_{30}) = \frac{E(A_{30}B_{30})}{30} - \frac{E(A_{36}B_{36})}{36} . \quad (6)$$

Notably, the $A_{30}B_{30}$ fullerenes are less stable than the $A_{36}B_{36}$ fullerenes for almost all element pairs studied (Figure 7). This observation is in stark contrast to carbon-based fullerenes where C_{60} is an exceptionally stable carbon allotrope[87-88]. Lighter elements, as exemplified by the three nitrogen-containing $A_{30}B_{30}$ fullerenes (A=boron, aluminum, gallium), favor the larger fullerene structure. For instance, these C_{60} analogues are destabilized by more than 11 kcal/mol per A/B atom pairs with respect to $A_{36}B_{36}$ fullerenes (see Supporting Information Table S9). Similarly,

the other two aluminum-containing $A_{30}B_{30}$ fullerenes (B=phosphorus, arsenic) are destabilized by more than 5 kcal/mol per A/B atom pair with respect to $A_{36}B_{36}$ fullerenes. For all 16 compounds considered, boron arsenide fullerenes are the only III-V material for which the $B_{30}As_{30}$ structure is more stable than $B_{36}As_{36}$. For II-VI materials, the $A_{30}B_{30}$ fullerenes are destabilized even further by about 10-14 kcal/mol per A/B pair with respect to the $A_{36}B_{36}$ compounds. This energetic trend is not primarily a size effect, as the stabilities of $A_{28}B_{28}$ fullerenes are comparable to $A_{36}B_{36}$ fullerenes, likely due to the presence only of even-membered A-B-alternating rings. One exception to this size-insensitivity is the nitrogen-containing $A_{28}B_{28}$ fullerenes, which have a relative energy of 2 kcal/mol per A/B pair higher compared to the larger $A_{36}B_{36}$ fullerenes.

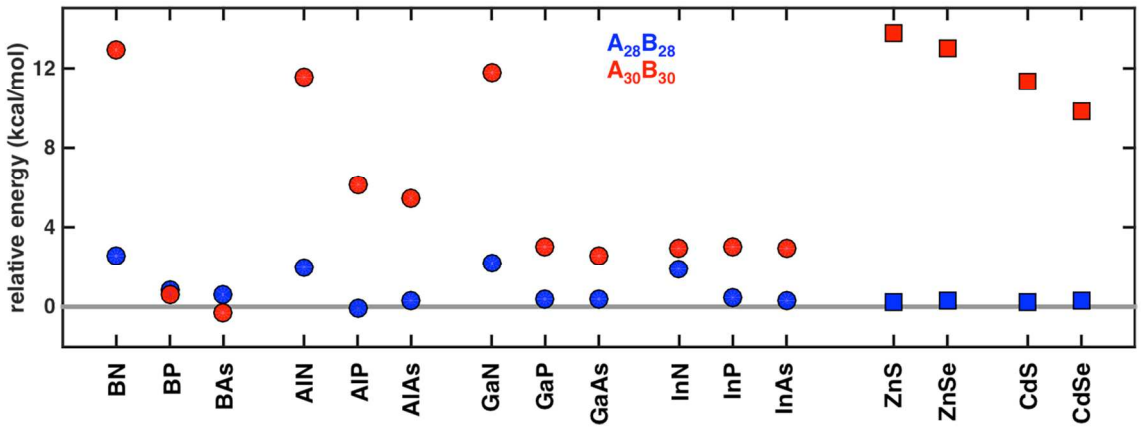

Figure 7. Relative energy per pair of A/B atoms in kcal/mol of geometry optimized $A_{28}B_{28}$ (blue) and $A_{30}B_{30}$ (red) fullerenes with respect to $A_{36}B_{36}$ fullerenes from III-V (circles) and II-VI (squares) materials.

We now examine the source of differences in relative stability of $A_{30}B_{30}$ and $A_{36}B_{36}$ fullerenes with quantitative measures derived from the structural and electronic properties of the materials. In order to determine structural effects, we built III-V and II-VI four-, five-, and six-

membered rings, passivated the structures with hydrogen atoms, and computed the relative energies of geometry-optimized four- and five-membered rings with respect to optimized six-membered rings (Figure 8). These energy penalties (E^4_{penalty} for four-membered rings and E^5_{penalty} for five-membered rings) are computed as follows:

$$E^4_{\text{penalty}} = 2\left[\frac{E(\text{A}_2\text{B}_2\text{H}_4)}{2} - \frac{E(\text{A}_3\text{B}_3\text{H}_6)}{3}\right], \quad \text{and} \tag{7}$$

$$E^5_{\text{penalty}} = \frac{5}{2}\left[\frac{E(\text{A}_3\text{B}_2\text{H}_5)}{5} + \frac{E(\text{A}_2\text{B}_3\text{H}_5)}{5} - \frac{E(\text{A}_3\text{B}_3\text{H}_6)}{3}\right], \tag{8}$$

where $E(\text{A}_2\text{B}_2\text{H}_4)$, $E(\text{A}_3\text{B}_2\text{H}_5)$, $E(\text{A}_2\text{B}_3\text{H}_5)$, $E(\text{A}_3\text{B}_3\text{H}_6)$ are the energies of optimized $\text{A}_2\text{B}_2\text{H}_4$ four-membered ring molecules, $\text{A}_3\text{B}_2\text{H}_5$ or $\text{A}_2\text{B}_3\text{H}_5$ five-membered ring molecules, and $\text{A}_3\text{B}_3\text{H}_6$ six-membered ring molecules. The energy penalties of both four- and five-membered rings decrease with increasingly heavy anion atoms, but the relative stability of four- and five-membered rings varies across the studied materials (Table 2). If bond strain is the largest factor, then four-membered ring energies will always be higher, whereas five-membered rings are expected to be unstable due to the lower favorability of nonpolar bonds with respect to their polar counterparts. The BN, AlN, AlP, AlAs and GaN materials penalize the five-membered ring structures more than four-membered rings, whereas all the other III-V materials show the reverse trend. In previous work[75], we identified P-P bonds to be favorable in amorphous InP clusters, consistent with a lower five-membered ring penalty than four-membered ring penalty in this material (see Table 2). The more ionic nature and larger size of the substituents in II-VI materials results in a much larger penalty for the nonpolar bond-containing five-membered ring structures and relatively small penalties for the four-membered rings.

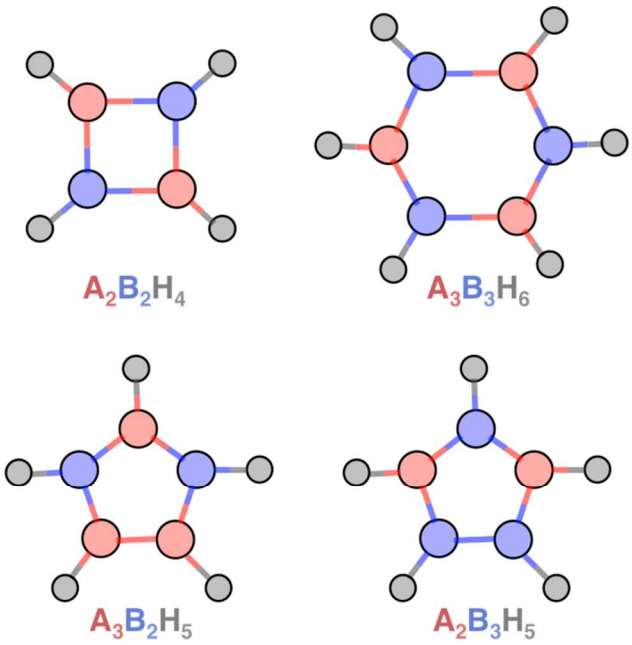

Figure 8. Representative ball-and-stick models of hydrogen-passivated four-, five-, six-membered rings: $A_2B_2H_4$ (top left), $A_3B_2H_5$ (bottom left), $A_2B_3H_5$ (bottom right), and $A_3B_3H_6$ (top right) with A atoms shown in red, B atoms in blue and H atoms in gray.

Table 2. Relative energy penalties of four-membered (E^4_{penalty}), and five-membered (E^5_{penalty}) rings with respect to six-membered rings in kcal/mol for III-V and II-VI materials.

	E^4_{penalty}	E^5_{penalty}		E^4_{penalty}	E^5_{penalty}
BN	51.1	58.2	GaAs	11.9	6.0
BP	33.9	18.2	InN	27.1	25.1
BAs	28.4	17.2	InP	19.2	10.6
AlN	29.4	49.8	InAs	17.8	13.9
AlP	19.8	21.8	ZnS	9.2	45.8
AlAs	18.9	20.0	ZnSe	5.4	37.4
GaN	31.0	44.5	CdS	6.8	39.0
GaP	20.7	15.7	CdSe	5.6	35.7

In addition to the relative energy penalty between differing ring structures, the quantity of each ring structure type also matters. In each $A_{30}B_{30}$ fullerene, there are 12 five-membered rings but each $A_{36}B_{36}$ fullerene only contains 6 four-membered rings. Therefore the relative penalties for $A_{30}B_{30}$ and $A_{36}B_{36}$ fullerenes should be calculated as a weighted difference in the number of unfavorable rings on a per-pair of atom basis to maintain consistency as follows:

$$\Delta E_{\text{penalty}} = \frac{12E^{5}_{\text{penalty}}}{30} - \frac{6E^{4}_{\text{penalty}}}{36}. \quad (9)$$

The relative $A_{30}B_{30}$ to $A_{36}B_{36}$ fullerene energies correlate very well (R^2=0.92) with the ring-derived energy penalty differences between the two structures (Figure 9). Therefore, our simplified ring model captures all of the underlying differences in chemical bonding that stabilize the $A_{36}B_{36}$ fullerene structures. Although for some heavier III-V materials, five-membered rings are more stable than four-membered rings, the larger (12 vs. 6) number of five-membered rings in $A_{30}B_{30}$ fullerenes with respect to four-membered rings in $A_{36}B_{36}$ means that the 72-atom fullerene is almost always favored. In order to test the transferability of our derived trend, we investigated whether the relative overall stability of group IV elemental A_{60} and A_{72} fullerenes (A=C, Si, or Ge) would correlate to the energy penalty differences based on their four-, five-, and six-membered rings (see Supporting Information Method S2 for details). Here, any penalty in the four- and five-membered rings should be derived solely from strain because all bonds are now nonpolar. Heavier A_{60} (A=Si, Ge) fullerenes follow the same trend as the heteronuclear materials, but our ring energy penalty metric slightly underestimates the stability of the lighter C_{60}. The difference comes from the underestimated energy penalty of the hydrogen-passivated four-membered ring because this isolated ring structure assumes an alternating single and double bond structure, but the four-membered rings in fullerenes all have

equivalent bond order. For the heavier group IV A_{60} (A=Si, Ge), the four-membered rings in the fullerene structures are twisted instead of flat, leading to a more representative energetic contribution from the isolated four-membered ring structure.

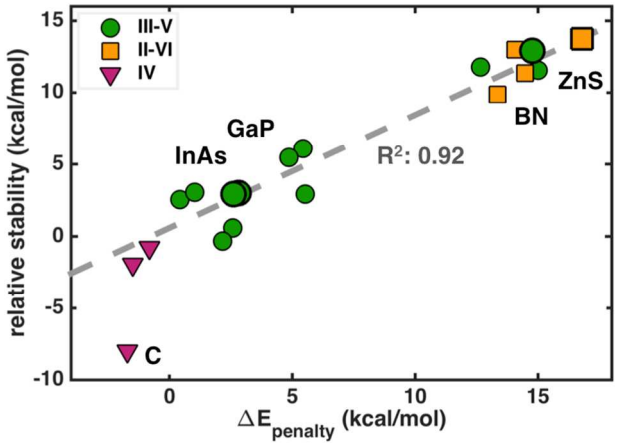

Figure 9. Relationship of the relative energy per pair of AB atoms in kcal/mol of $A_{30}B_{30}$ fullerenes referenced against $A_{36}B_{36}$ fullerenes from III-V (green circles), II-VI (orange squares), and IV (magenta triangles) materials with energy penalty differences per pair of AB atoms in kcal/mol between $A_{30}B_{30}$ and $A_{36}B_{36}$ fullerenes. A best-fit line (gray dashed) fit only to III-V and II-VI data is shown. Select labeled compounds are highlighted with bolder symbols.

We also used a reference $A_{36}B_{36}$ spherical nanoparticle to directly compare stabilities of the three different fullerene geometries with respect to substituent cation or anion element changes. We calculate the relative energy per AB pair in three optimized fullerenes $E(A_nB_n)$ (n=28, 30, or 36) with respect to those in the optimized $A_{36}B_{36}$ NP (E(NP)) as:

$$E_{\text{per pair}}(\text{FL}) = \frac{E(\text{A}_\text{n}\text{B}_\text{n})}{n} - \frac{E(\text{NP})}{36} \quad . \tag{10}$$

We then examined possible correlations between the relative energies of each fullerene structure with all previously studied materials property descriptors of underlying atoms (e.g., electronegativity or covalent radius) and structure-specific properties (e.g., four- or five-membered rings). From several combinations, we obtained a descriptor, β, which is correlated to the relative stability for all three fullerene structures:

$$\beta = 18.17(r_{\text{cov}}^{\text{A}} + r_{\text{cov}}^{\text{B}}) + \frac{1}{41}(0.19 n_4 E_{\text{penalty}}^4 + 0.81 n_5 E_{\text{penalty}}^5) - 0.06 n_6, \quad (11)$$

where $r_{\text{cov}}^{\text{A}}$ and $r_{\text{cov}}^{\text{B}}$ are covalent radii of A and B atoms in □, n_4, n_5, n_6 are number of four-, five-, six-membered rings in the fullerenes, and E_{penalty}^4, E_{penalty}^5 are energy penalties of four-, five-membered rings in kcal/mol. The relative stability of each fullerene ($E_{\text{per pair}}$(FL)) is correlated to the descriptor β (Figure 10):

$$E_{\text{per pair}}(\text{FL}) = \beta - 43.4, \quad (12)$$

where the constant -43.4 kcal/mol depends on the chosen reference structure (an $A_{36}B_{36}$ NP). The quantities present in our β descriptor are an intuitive mixture of size- and structure-dependent properties. The relative energy of a fullerene increases with covalent radii of A, B atoms or total energy penalties of four-, five-membered rings, but it decreases with increasing structure size, as indicated by the number of six-membered rings. The instability caused by the energy penalty of five-membered rings is four times larger than that of four-membered rings, as indicated by weights in the final expression and thus this more general correlation indicates that nonpolar bonding is even more destabilizing in the general data set than in our original penalty vs. stability correlation. The size effect corresponding to the number of six-membered rings has a small

influence on the fullerene stability, suggesting topology of the fullerene, as described by constituent ring structure energetics, is much more relevant than the size.

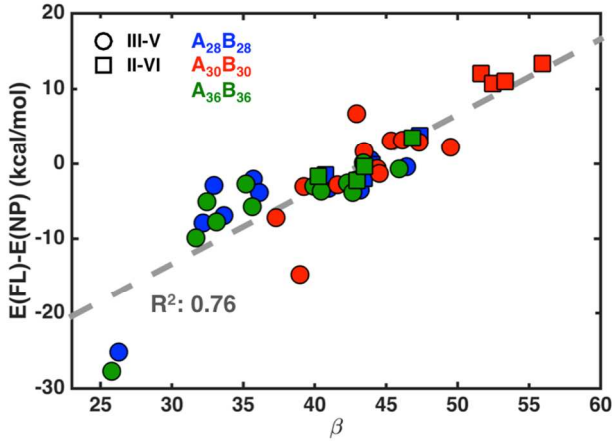

Figure 10. Relationship of relative energy per pair of AB atoms in kcal/mol of $A_{28}B_{28}$ (blue), $A_{30}B_{30}$ (red), and $A_{36}B_{36}$ (green) fullerenes referenced against the $A_{36}B_{36}$ spherical nanoparticles from III-V (circles) and II-V (squares) materials with a descriptor β which is a linear combination of sum of covalent radius of A and B atoms, total energy penalties of four-, five-membered rings, and number of six-membered rings (the form of β is shown in text). A best-fit line (gray dashed) is also shown.

4. Conclusions

We have carried out a systematic study of the role of elemental identity in determining electronic, energetic, and geometric properties of prototypical (i.e., $A_{28}B_{28}$, $A_{30}B_{30}$, and $A_{36}B_{36}$) III-V and II-VI fullerene allotropes. Our use of a nanoparticle reference enabled identification of potentially stable $Al_{36}N_{36}$, $Ga_{36}N_{36}$, $In_{36}N_{36}$, and $B_{36}P_{36}$ fullerenes in addition to the previously-characterized $B_{36}N_{36}$. We found a suitable composite descriptor of electronegativity differences

and sum of covalent radii that captured relative fullerene stability in these materials, and, importantly, this descriptor is transferable to group IV A_{72} fullerenes. We observed a shift in band gap with increasingly heavy cation or anion substitutions in the $A_{36}B_{36}$ fullerenes, as well as shifts in the dominant anion atom *p* orbitals in valence band and dominant cation atom *p* orbitals in conduction band, which can be explained by analyzing the NBO partial charges for the fullerenes. Our analysis of chemical bonding in these fullerenes revealed a log-log relation between bonding orbital contributions from A atoms in localized orbitals and the electronegativity differences between A and B atoms.

We next investigated differences between the 72-atom fullerenes and their $A_{30}B_{30}$ Buckminsterfullerene counterparts, where the latter contain covalent, nonpolar bonds due to the presence of five-membered rings absent in the former, which consists only of polar, alternating A-B bonds in four- and six-membered rings. We expected the four-membered rings of $A_{36}B_{36}$ fullerenes to reduce overall stability due to their large strain energy, but we also anticipated that the nonpolar bonds in $A_{30}B_{30}$ fullerenes might be energetically unfavorable. We found the strain effect to be smaller than the penalty for nonpolar bonding, as $A_{30}B_{30}$ fullerenes were less stable than the $A_{36}B_{36}$ fullerenes for almost all element pairs studied. We also considered size effects by comparison to a smaller $A_{28}B_{28}$ fullerene model, which contains solely four- and six-membered rings and found the energetic trend to not be strongly size-dependent, as the stabilities of $A_{28}B_{28}$ fullerenes are comparable to $A_{36}B_{36}$ fullerenes. In order to understand the energetic difference, we constructed hydrogen-passivated four-, five-, and six-membered rings and computed energy penalties of the strain effect and nonpolar bonds induced by four- and five-membered rings, respectively. We observed a strong correlation between the total relative energy penalties of these substituent ring models to relative fullerene energies. A simple descriptor that

consisted only of these penalties and a measure of element size via covalent radii correlated well to the stabilities of all three fullerene allotropes. Overall, our study has demonstrated a path forward for predicting the relative stability of additional fullerene allotropes of arbitrary shape and size. The strategy presented here should be useful in identifying new stable element combinations and doping strategies in fullerenes.

ASSOCIATED CONTENT

Supporting Information.

Supporting Information is available free of charge via the Internet at http://pubs.acs.org. Distance cutoffs for A-B bonds and electronegativity differences of B, A elements; initial configurations of $A_{36}B_{36}$ nanoparticles; geometry parameters (bond distances of $A_{36}B_{36}$, $A_{28}B_{28}$, $A_{30}B_{30}$ fullerenes, CN of $A_{36}B_{36}$ nanoparticles); stability analysis of $A_{36}B_{36}$ fullerenes; experimental band gap of AB crystals; electronic properties of $A_{36}B_{36}$ fullerenes (HOMO, LUMO, CB, VB, PDOS, NBO charge); relative energy of $A_{28}B_{28}$, $A_{30}B_{30}$ fullerenes; methods to build, compute relative stability, and analyze A_{72} and A_{60} fullerenes.

AUTHOR INFORMATION

Corresponding Author

*email: hjkulik@mit.edu phone: 617-253-4584

Notes

The authors declare no competing financial interest.

ACKNOWLEDGMENT

This work was supported by the National Science Foundation under grant number ECCS-1449291. H.J.K. holds a Career Award at the Scientific Interface from the Burroughs Wellcome Fund. This work was carried out in part using computational resources from the Extreme Science and Engineering Discovery Environment (XSEDE), which is supported by National Science Foundation grant number ACI-1053575. The authors would like to thank Helena W. Qi and Adam H. Steeves for providing a critical reading of the manuscript.

REFERENCES

1. Kroto, H. W.; Heath, J. R.; O'Brien, S. C.; Curl, R. F.; Smalley, R. E., C 60: buckminsterfullerene. *Nature* **1985**, *318*, 162-163.
2. Hirsch, A., The era of carbon allotropes. *Nat. Mater.* **2010**, *9*, 868-871.
3. Campoy-Quiles, M.; Ferenczi, T.; Agostinelli, T.; Etchegoin, P. G.; Kim, Y.; Anthopoulos, T. D.; Stavrinou, P. N.; Bradley, D. D.; Nelson, J., Morphology evolution via self-organization and lateral and vertical diffusion in polymer: fullerene solar cell blends. *Nat. Mater.* **2008**, *7*, 158-164.
4. Vandewal, K.; Tvingstedt, K.; Gadisa, A.; Inganäs, O.; Manca, J. V., On the origin of the open-circuit voltage of polymer–fullerene solar cells. *Nat. Mater.* **2009**, *8*, 904-909.
5. Price, S. C.; Stuart, A. C.; Yang, L.; Zhou, H.; You, W., Fluorine substituted conjugated polymer of medium band gap yields 7% efficiency in polymer− fullerene solar cells. *J. Am. Chem. Soc.* **2011**, *133*, 4625-4631.
6. Scharber, M. C., On the Efficiency Limit of Conjugated Polymer: Fullerene□Based Bulk Heterojunction Solar Cells. *Adv. Mater* **2016**, *28*, 1994-2001.
7. Zakharian, T. Y.; Seryshev, A.; Sitharaman, B.; Gilbert, B. E.; Knight, V.; Wilson, L. J., A fullerene-paclitaxel chemotherapeutic: synthesis, characterization, and study of biological activity in tissue culture. *J. Am. Chem. Soc.* **2005**, *127*, 12508-12509.
8. Shi, J.; Zhang, H.; Wang, L.; Li, L.; Wang, H.; Wang, Z.; Li, Z.; Chen, C.; Hou, L.; Zhang, C., PEI-derivatized fullerene drug delivery using folate as a homing device targeting to tumor. *Biomaterials* **2013**, *34*, 251-261.
9. Yoon, M.; Yang, S.; Hicke, C.; Wang, E.; Geohegan, D.; Zhang, Z., Calcium as the superior coating metal in functionalization of carbon fullerenes for high-capacity hydrogen storage. *Phys. Rev. Lett.* **2008**, *100*, 206806.
10. Chuvilin, A.; Kaiser, U.; Bichoutskaia, E.; Besley, N. A.; Khlobystov, A. N., Direct transformation of graphene to fullerene. *Nat. Chem.* **2010**, *2*, 450-453.

11. Aoyagi, S.; Nishibori, E.; Sawa, H.; Sugimoto, K.; Takata, M.; Miyata, Y.; Kitaura, R.; Shinohara, H.; Okada, H.; Sakai, T., A layered ionic crystal of polar Li@ C60 superatoms. *Nat. Chem.* **2010**, *2*, 678-683.
12. Golberg, D.; Bando, Y.; Stephan, O.; Kurashima, K., Octahedral boron nitride fullerenes formed by electron beam irradiation. *Appl. Phys.* **1998**, *73*, 2441.
13. Oku, T.; Nishiwaki, A.; Narita, I., Formation and atomic structure of B 12 N 12 nanocage clusters studied by mass spectrometry and cluster calculation. *Sci. Technol. Adv. Mater.* **2004**, *5*, 635-638.
14. Oku, T.; Nishiwaki, A.; Narita, I.; Gonda, M., Formation and structure of B 24 N 24 clusters. *Chem. Phys.* **2003**, *380*, 620-623.
15. Oku, T.; Nishiwaki, A.; Narita, I., Formation and atomic structures of B n N n (n= 24–60) clusters studied by mass spectrometry, high-resolution electron microscopy and molecular orbital calculations. *Phys. B* **2004**, *351*, 184-190.
16. Oku, T.; Kuno, M.; Narita, I., High-resolution electron microscopy and electronic structures of endohedral La@ B 36 N 36 clusters. *Diamond Relat. Mater.* **2002**, *11*, 940-944.
17. Oku, T.; Narita, I.; Nishiwaki, A., Formation and structures of B 36 N 36 and Y@ B 36 N 36 clusters studied by high-resolution electron microscopy and mass spectrometry. *J. Phys. Chem. Solids* **2004**, *65*, 369-372.
18. Ogitsu, T.; Schwegler, E.; Galli, G., β-Rhombohedral Boron: At the Crossroads of the Chemistry of Boron and the Physics of Frustration. *Chem. Rev.* **2013**, *113*, 3425-3449.
19. White, M. A.; Cerqueira, A. B.; Whitman, C. A.; Johnson, M. B.; Ogitsu, T., Determination of phase stability of elemental boron. *Angew. Chem.* **2015**, *127*, 3697-3700.
20. Zhai, H.-J.; Zhao, Y.-F.; Li, W.-L.; Chen, Q.; Bai, H.; Hu, H.-S.; Piazza, Z. A.; Tian, W.-J.; Lu, H.-G.; Wu, Y.-B., Observation of an all-boron fullerene. *Nat. Chem.* **2014**, *6*, 727-731.
21. Etzkorn, J.; Therese, H. A.; Rocker, F.; Zink, N.; Kolb, U.; Tremel, W., Metal–Organic Chemical Vapor Depostion Synthesis of Hollow Inorganic□Fullerene□Type MoS2 and MoSe2 Nanoparticles. *Adv. Mater* **2005**, *17*, 2372-2375.
22. Sadan, M. B.; Houben, L.; Enyashin, A. N.; Seifert, G.; Tenne, R., Atom by atom: HRTEM insights into inorganic nanotubes and fullerene-like structures. *Proc. Natl. Acad. Sci.* **2008**, *105*, 15643-15648.
23. Albu□Yaron, A.; Levy, M.; Tenne, R.; Popovitz□Biro, R.; Weidenbach, M.; Bar□Sadan, M.; Houben, L.; Enyashin, A. N.; Seifert, G.; Feuermann, D., MoS2 Hybrid Nanostructures: From Octahedral to Quasi□Spherical Shells within Individual Nanoparticles. *Angew. Chem. Int. Ed.* **2011**, *50*, 1810-1814.
24. Wu, H.; Yang, R.; Song, B.; Han, Q.; Li, J.; Zhang, Y.; Fang, Y.; Tenne, R.; Wang, C., Biocompatible inorganic fullerene-like molybdenum disulfide nanoparticles produced by pulsed laser ablation in water. *ACS Nano* **2011**, *5*, 1276-1281.
25. Moon, W. H.; Son, M. S.; Hwang, H. J., Theoretical study on structure of boron nitride fullerenes. *Appl. Surf. Sci.* **2007**, *253*, 7078-7081.
26. Wu, H.-S.; Xu, X.-H.; Strout, D. L.; Jiao, H., The structure and stability of B36N36 cages: a computational study. *J. Mol. Model.* **2005**, *12*, 1-8.
27. Barone, V.; Koller, A.; Scuseria, G. E., Theoretical nitrogen NMR chemical shifts in octahedral boron nitride cages. *J. Phys. Chem. A* **2006**, *110*, 10844-10847.
28. Batista, R. J.; Mazzoni, M. S.; Chacham, H., A theoretical study of the stability trends of boron nitride fullerenes. *Chem. Phys.* **2006**, *421*, 246-250.

29. Wu, H.-S.; Cui, X.-Y.; Qin, X.-F.; Strout, D. L.; Jiao, H., Boron nitride cages from B12N12 to B36N36: square–hexagon alternants vs boron nitride tubes. *J. Mol. Model.* **2006**, *12*, 537-542.
30. Batista, R. J.; Mazzoni, M. S.; Chacham, H., Boron nitride fullerene B 36 N 36 doped with transition metal atoms: First-principles calculations. *Phys. Rev. B* **2007**, *75*, 035417.
31. Koponen, L.; Tunturivuori, L.; Puska, M. J.; Nieminen, R. M., Photoabsorption spectra of boron nitride fullerenelike structures. *J. Chem. Phys.* **2007**, *126*, 214306.
32. Matxain, J. M.; Eriksson, L. A.; Mercero, J. M.; Lopez, X.; Piris, M.; Ugalde, J. M.; Poater, J.; Matito, E.; Solá, M., New solids based on B12N12 fullerenes. *J. Phys. Chem. C* **2007**, *111*, 13354-13360.
33. Karttunen, A. J.; Linnolahti, M.; Pakkanen, T. A., Structural Characteristics of Perhydrogenated Boron Nitride Fullerenes. *J. Phys. Chem. C* **2008**, *112*, 10032-10037.
34. Beheshtian, J.; Bagheri, Z.; Kamfiroozi, M.; Ahmadi, A., A comparative study on the B12N12, Al12N12, B12P12 and Al12P12 fullerene-like cages. *J. Mol. Model.* **2012**, *18*, 2653-2658.
35. Pokropivny, V.; Ovsyannikova, L., Electronic structure and the infrared absorption and Raman spectra of the semiconductor clusters C24, B12N12, Si12C12, Zn12O12, and Ga12N12. *Phys. Solid State* **2007**, *49*, 562-570.
36. Zope, R. R.; Dunlap, B. I., Electronic structure of fullerenelike cages and finite nanotubes of aluminum nitride. *Phys. Rev. B* **2005**, *72*, 045439.
37. Wang, B.; Wang, X.; Chen, G.; Nagase, S.; Zhao, J., Cage and tube structures of medium-sized zinc oxide clusters (ZnO) n (n= 24, 28, 36, and 48). *J. Chem. Phys.* **2008**, *128*, 144710.
38. Yong, Y.; Li, X.; Hao, X.; Cao, J.; Li, T., Theoretical prediction of low-density nanoporous frameworks of zinc sulfide based on Zn n S n (n= 12, 16) nanocaged clusters. *RSC Adv.* **2014**, *4*, 37333-37341.
39. Niu, M.; Yu, G.; Yang, G.; Chen, W.; Zhao, X.; Huang, X., Doping the Alkali Atom: An Effective Strategy to Improve the Electronic and Nonlinear Optical Properties of the Inorganic Al12N12 Nanocage. *Inorg. Chem.* **2013**, *53*, 349-358.
40. Shakerzadeh, E.; Barazesh, N.; Talebi, S. Z., A comparative theoretical study on the structural, electronic and nonlinear optical features of B 12 N 12 and Al 12 N 12 nanoclusters with the groups III, IV and V dopants. *Superlattices and Microstructures* **2014**, *76*, 264-276.
41. Rad, A. S.; Ayub, K., Ni adsorption on Al 12 P 12 nano-cage: A DFT study. *J. Alloys Compd.* **2016**, *678*, 317-324.
42. Lu, P.; Wu, C.; Li, Y.; Yu, Z.; Cao, H.; Wang, S., Investigation on structural, electronic, and magnetic properties of Mn-doped Ga12N12 clusters. *J. Mater. Sci.* **2013**, *48*, 8552-8558.
43. Peyghan, A. A.; Pashangpour, M.; Bagheri, Z.; Kamfiroozi, M., Energetic, structural, and electronic properties of hydrogenated Al 12 P 12 nanocluster. *Phys. E* **2012**, *44*, 1436-1440.
44. Beheshtian, J.; Kamfiroozi, M.; Bagheri, Z.; Ahmadi, A., Theoretical study of hydrogen adsorption on the B 12 P 12 fullerene-like nanocluster. *Comput. Mater. Sci.* **2012**, *54*, 115-118.
45. Yong, Y.; Song, B.; He, P., Cluster-assembled materials based on M 12 N 12 (M= Al, Ga) fullerene-like clusters. *Phys. Chem. Chem. Phys.* **2011**, *13*, 16182-16189.
46. Yong, Y.; Song, B.; He, P., Growth pattern and electronic properties of cluster-assembled material based on Zn12O12: A density-functional study. *J. Phys. Chem. C* **2011**, *115*, 6455-6461.

47. Ghosh, S.; Sanyal, B.; Das, G., Structural, electronic and magnetic properties of Cr-doped Cd 12 S 12 clusters: A density functional investigation. *J. Magn. Magn. Mater.* **2010**, *322*, 734-742.
48. Küskü, S. İ.; Berber, S., Stability of Ga x As x±4 gallium arsenide fullerenes. *Phys. Rev. B* **2009**, *79*, 245420.
49. Karamanis, P.; Pouchan, C., On the shape dependence of cluster (hyper) polarizabilities. A combined ab initio and DFT study on large fullerene–like gallium arsenide semiconductor clusters. *Int. J. Quantum Chem.* **2011**, *111*, 788-796.
50. Szwacki, N. G.; Sadrzadeh, A.; Yakobson, B. I., B 80 fullerene: an ab initio prediction of geometry, stability, and electronic structure. *Phys. Rev. Lett.* **2007**, *98*, 166804.
51. De, S.; Willand, A.; Amsler, M.; Pochet, P.; Genovese, L.; Goedecker, S., Energy landscape of fullerene materials: a comparison of boron to boron nitride and carbon. *Phys. Rev. Lett.* **2011**, *106*, 225502.
52. Beheshtian, J.; Kamfiroozi, M.; Bagheri, Z.; Peyghan, A. A., B12N12 nano-cage as potential sensor for NO2 detection. *Chin. J. Chem. Phys.* **2012**, *25*, 60-64.
53. Beheshtian, J.; Bagheri, Z.; Kamfiroozi, M.; Ahmadi, A., Toxic CO detection by B 12 N 12 nanocluster. *Microelectron. J.* **2011**, *42*, 1400-1403.
54. Hadipour, N. L.; Ahmadi Peyghan, A.; Soleymanabadi, H., Theoretical Study on the Al-Doped ZnO Nanoclusters for CO Chemical Sensors. *J. Phys. Chem. C* **2015**, *119*, 6398-6404.
55. Baei, M. T.; Tabar, M. B.; Hashemian, S., Zn12O12 Fullerene-like Cage as a Potential Sensor for SO2 Detection. *Adsorpt. Sci. Technol.* **2013**, *31*, 469-476.
56. Ghenaatian, H.; Baei, M. T.; Hashemian, S., Zn 12 O 12 nano-cage as a promising adsorbent for CS 2 capture. *Superlattices and Microstructures* **2013**, *58*, 198-204.
57. Ganji, M.; Yazdani, H.; Mirnejad, A., B 36 N 36 Fullerene-like nanocages: a novel material for drug delivery. *Phys. E* **2010**, *42*, 2184-2189.
58. Li, M.; Li, Y.; Zhou, Z.; Shen, P.; Chen, Z., Ca-coated boron fullerenes and nanotubes as superior hydrogen storage materials. *Nano Lett.* **2009**, *9*, 1944-1948.
59. Venkataramanan, N. S.; Belosludov, R. V.; Note, R.; Sahara, R.; Mizuseki, H.; Kawazoe, Y., Theoretical investigation on the alkali-metal doped BN fullerene as a material for hydrogen storage. *Chem. Phys.* **2010**, *377*, 54-59.
60. Wu, H.; Fan, X.; Kuo, J.-L., Metal free hydrogenation reaction on carbon doped boron nitride fullerene: A DFT study on the kinetic issue. *Int. J. Hydrogen Energy* **2012**, *37*, 14336-14342.
61. Wang, G.; Yuan, H.; Kuang, A.; Hu, W.; Zhang, G.; Chen, H., High-capacity hydrogen storage in Li-decorated (AlN) n (n= 12, 24, 36) nanocages. *Int. J. Hydrogen Energy* **2014**, *39*, 3780-3789.
62. Zhang, Y.; Zheng, X.; Zhang, S.; Huang, S.; Wang, P.; Tian, H., Bare and Ni decorated Al 12 N 12 cage for hydrogen storage: A first-principles study. *Int. J. Hydrogen Energy* **2012**, *37*, 12411-12419.
63. Petachem. http://www.petachem.com. (accessed Apr 28, 2016).
64. Ufimtsev, I. S.; Martinez, T. J., Quantum chemistry on graphical processing units. 3. Analytical energy gradients, geometry optimization, and first principles molecular dynamics. *J. Chem. Theory Comput.* **2009**, *5*, 2619-2628.
65. Kästner, J.; Carr, J. M.; Keal, T. W.; Thiel, W.; Wander, A.; Sherwood, P., DL-FIND: An Open-Source Geometry Optimizer for Atomistic Simulations. *J. Phys. Chem. A* **2009**, *113*, 11856-11865.

66. Rohrdanz, M. A.; Martins, K. M.; Herbert, J. M., A long-range-corrected density functional that performs well for both ground-state properties and time-dependent density functional theory excitation energies, including charge-transfer excited states. *J. Chem. Phys.* **2009**, *130*, 054112.
67. Dovesi, R.; Orlando, R.; Erba, A.; Zicovich□Wilson, C. M.; Civalleri, B.; Casassa, S.; Maschio, L.; Ferrabone, M.; De La Pierre, M.; D'Arco, P., CRYSTAL14: A program for the ab initio investigation of crystalline solids. *Int. J. Quantum Chem.* **2014**, *114*, 1287-1317.
68. Gražulis, S.; Daškevič, A.; Merkys, A.; Chateigner, D.; Lutterotti, L.; Quirós, M.; Serebryanaya, N. R.; Moeck, P.; Downs, R. T.; Le Bail, A., Crystallography Open Database (COD): an open-access collection of crystal structures and platform for world-wide collaboration. *Nucleic Acids Res.* **2012**, *40*, D420-D427.
69. Tomanek, D. T., David http://www.nanotube.msu.edu/fullerene/fullerene-isomers.html. (accessed Apr 28, 2016).
70. Hanwell, M. D.; Curtis, D. E.; Lonie, D. C.; Vandermeersch, T.; Zurek, E.; Hutchison, G. R., Avogadro: An advanced semantic chemical editor, visualization, and analysis platform. *J. Cheminform.* **2012**, *4*, 17.
71. E. D. Glendening, J., K. Badenhoop, A. E. Reed, J. E. Carpenter, J. A. Bohmann, C. M. Morales, C. R. Landis, and F. Weinhold, NBO, version 6.0. 2013.
72. Pauling, L., The nature of the chemical bond. IV. The energy of single bonds and the relative electronegativity of atoms. *J. Am. Chem. Soc.* **1932**, *54*, 3570-3582.
73. Kilina, S. V.; Kilin, D. S.; Prezhdo, O. V., Breaking the phonon bottleneck in PbSe and CdSe quantum dots: Time-domain density functional theory of charge carrier relaxation. *ACS Nano* **2008**, *3*, 93-99.
74. Isborn, C. M.; Kilina, S. V.; Li, X.; Prezhdo, O. V., Generation of multiple excitons in PbSe and CdSe quantum dots by direct photoexcitation: first-principles calculations on small PbSe and CdSe clusters. *J. Phys. Chem. C* **2008**, *112*, 18291-18294.
75. Zhao, Q.; Xie, L.; Kulik, H. J., Discovering Amorphous Indium Phosphide Nanostructures with High-Temperature Ab Initio Molecular Dynamics. *Journal of Physical Chemistry C* **2015**, *119*, 23238–23249.
76. Sham, L.; Schlüter, M., Density-functional theory of the energy gap. *Phys. Rev. Lett.* **1983**, *51*, 1888.
77. Cohen, A. J.; Mori-Sánchez, P.; Yang, W., Fractional charge perspective on the band gap in density-functional theory. *Phys. Rev. B* **2008**, *77*, 115123.
78. Kümmel, S.; Kronik, L., Orbital-dependent density functionals: Theory and applications. *Rev. Mod. Phys.* **2008**, *80*, 3.
79. Kronik, L.; Stein, T.; Refaely-Abramson, S.; Baer, R., Excitation gaps of finite-sized systems from optimally tuned range-separated hybrid functionals. *J. Chem. Theory Comput.* **2012**, *8*, 1515-1531.
80. NIST. http://webbook.nist.gov/chemistry/. (accessed Apr 28, 2016).
81. Beheshtian, J.; Peyghan, A. A.; Bagheri, Z., Functionalization of [60] fullerene with butadienes: A DFT study. *Appl. Surf. Sci.* **2012**, *258*, 8980-8984.
82. Beu, T. A.; Onoe, J.; Hida, A., First-principles calculations of the electronic structure of one-dimensional C 60 polymers. *Phys. Rev. B* **2005**, *72*, 155416.
83. Shevlin, S.; Guo, Z.; Van Dam, H.; Sherwood, P.; Catlow, C. A.; Sokol, A.; Woodley, S., Structure, optical properties and defects in nitride (III–V) nanoscale cage clusters. *Phys. Chem. Chem. Phys.* **2008**, *10*, 1944-1959.

84. Vurgaftman, I.; Meyer, J.; Ram-Mohan, L., Band parameters for III–V compound semiconductors and their alloys. *J. Appl. Phys.* **2001**, *89*, 5815-5875.
85. Madelung, O., *Semiconductors: data handbook*; Springer Science & Business Media, 2012.
86. Kamal, C.; Chakrabarti, A.; Ezawa, M., Direct Band Gaps in Group IV-VI Monolayer Materials: Binary Counterparts of Phosphorene. *arXiv preprint arXiv:1512.07598* **2015**.
87. Wales, D. J.; Miller, M. A.; Walsh, T. R., Archetypal energy landscapes. *Nature* **1998**, *394*, 758-760.
88. Ewels, C. P.; Rocquefelte, X.; Kroto, H. W.; Rayson, M. J.; Briddon, P. R.; Heggie, M. I., Predicting experimentally stable allotropes: Instability of penta-graphene. *Proc. Natl. Acad. Sci.* **2015**, *112*, 15609-15612.

TOC graphic

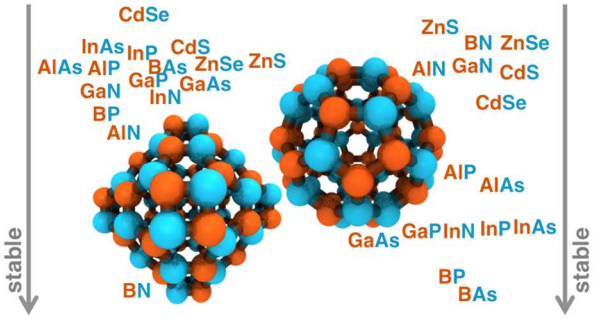

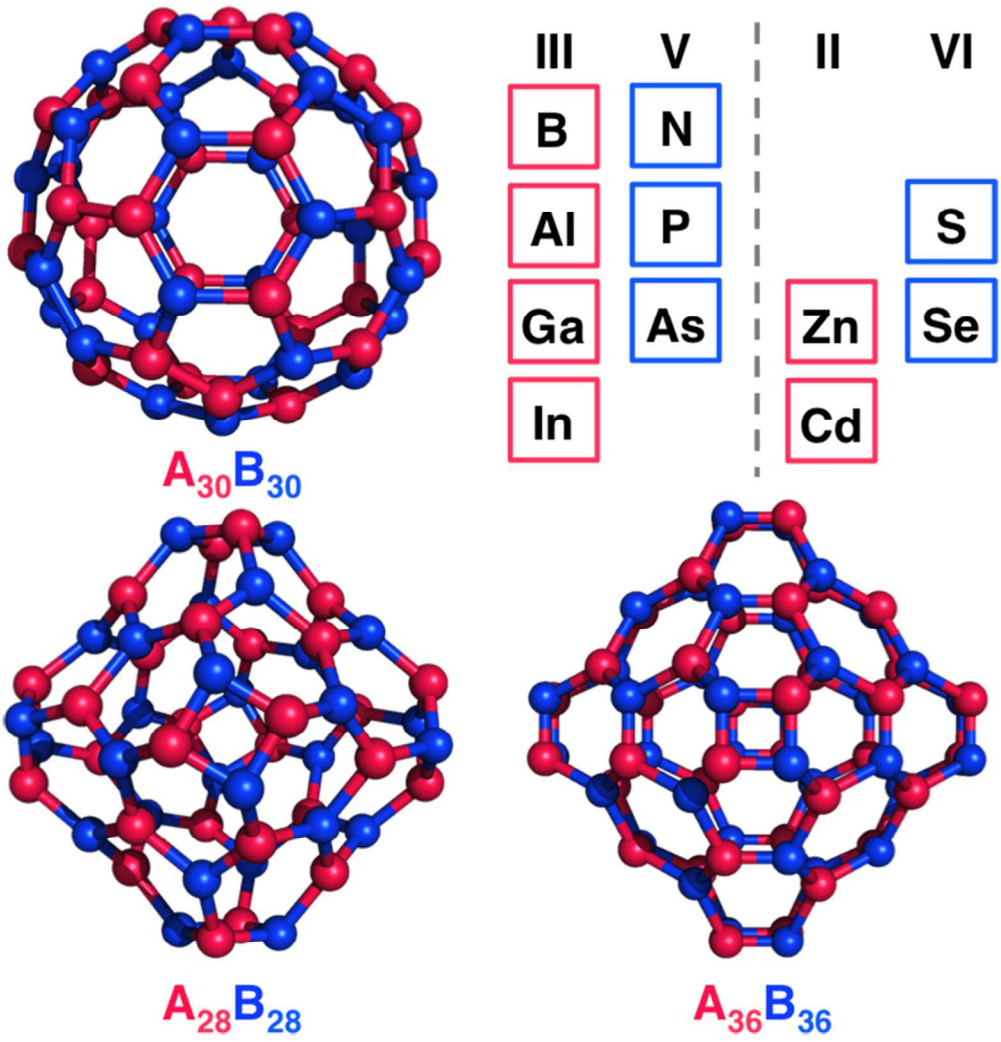

82x85mm (300 x 300 DPI)

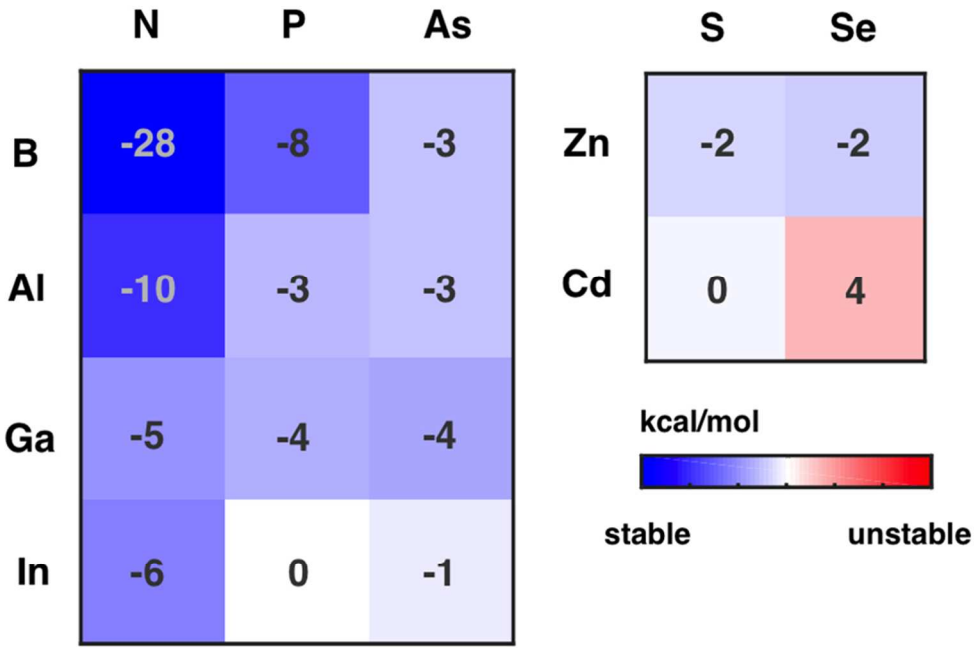

82x55mm (300 x 300 DPI)

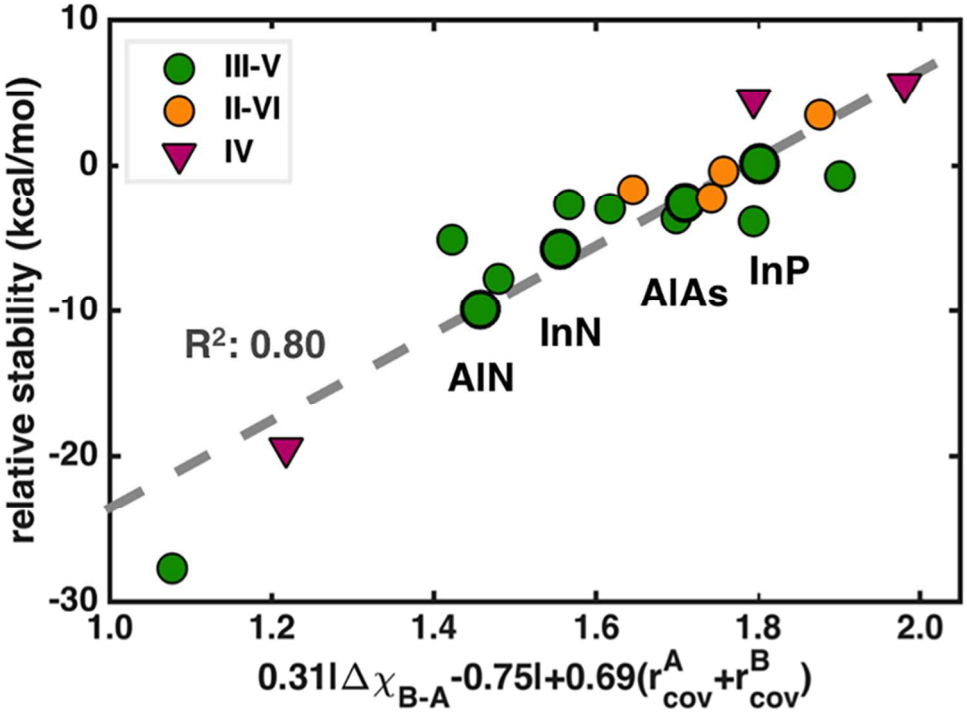

82x59mm (300 x 300 DPI)

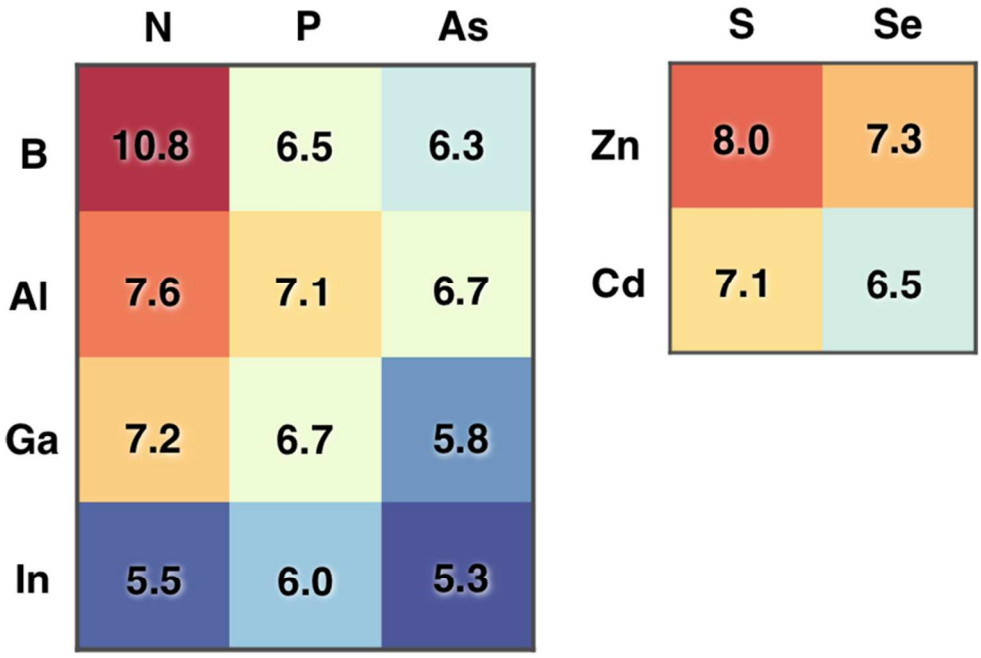

82x56mm (300 x 300 DPI)

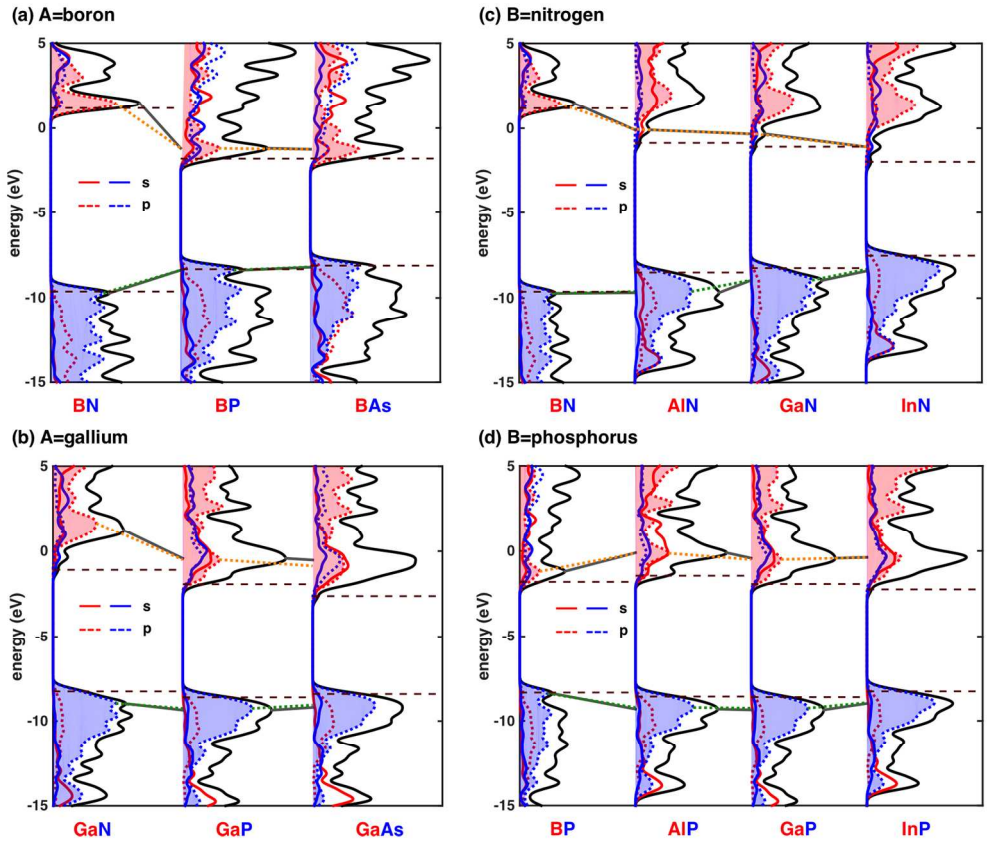

165x140mm (300 x 300 DPI)

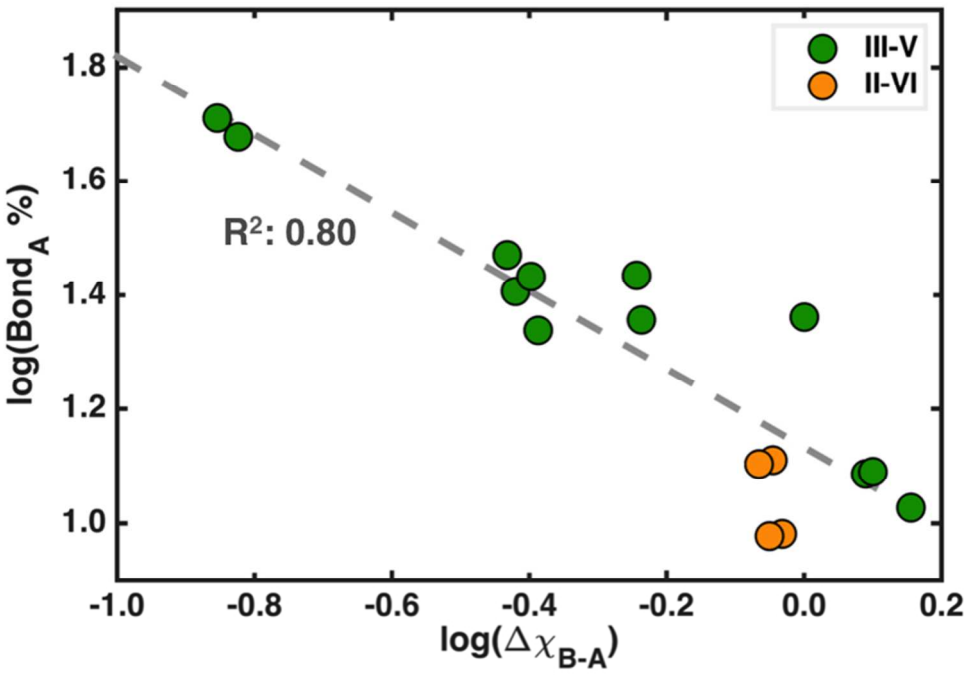

82x56mm (300 x 300 DPI)

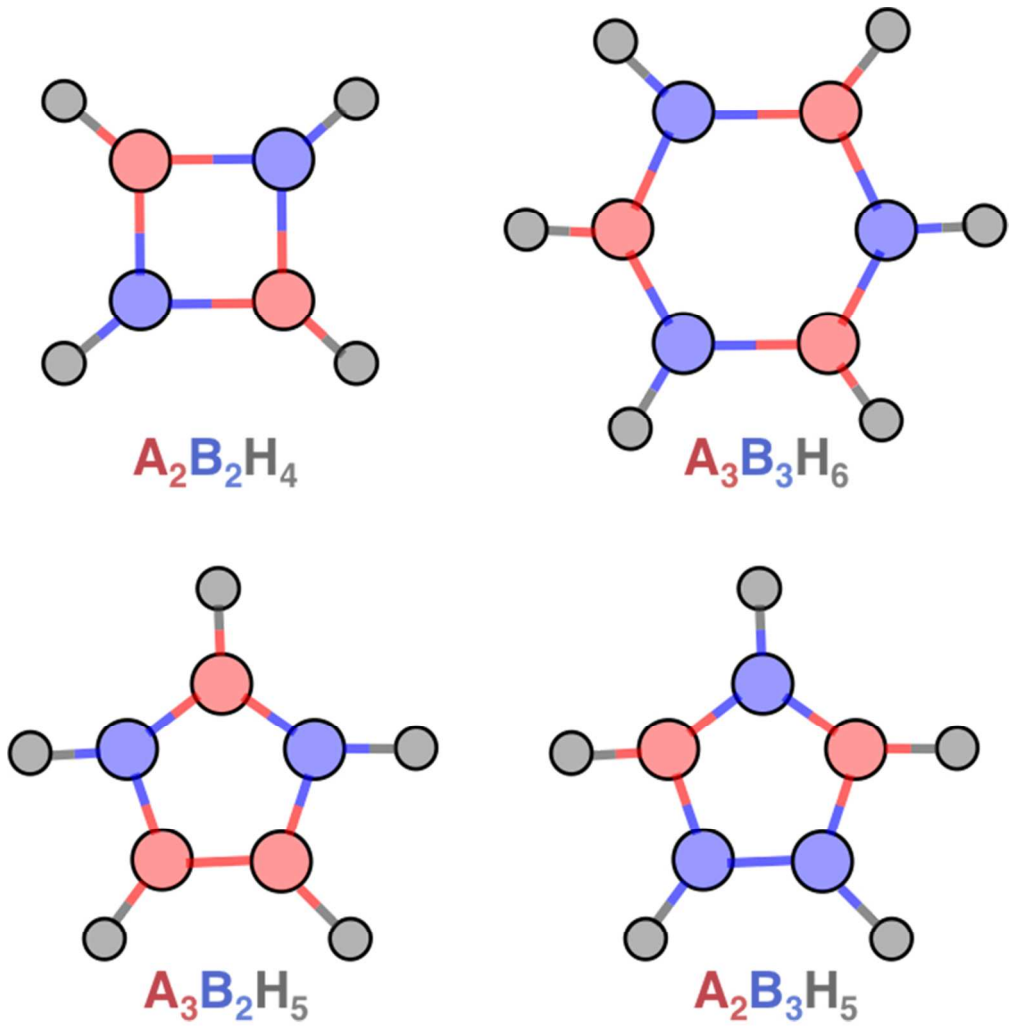

82x84mm (300 x 300 DPI)

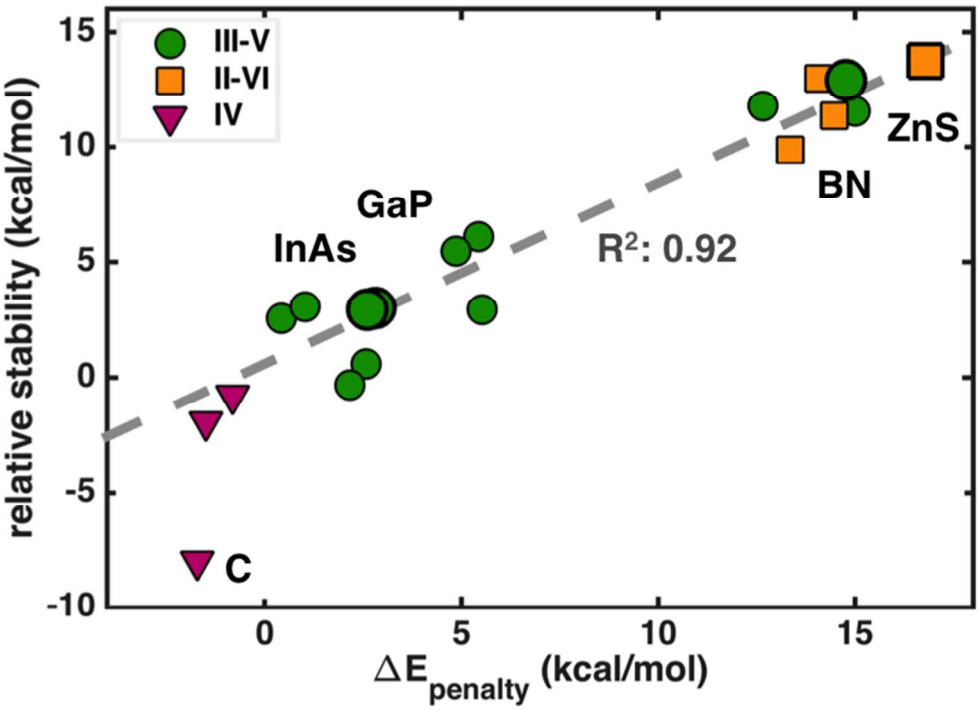

82x58mm (300 x 300 DPI)

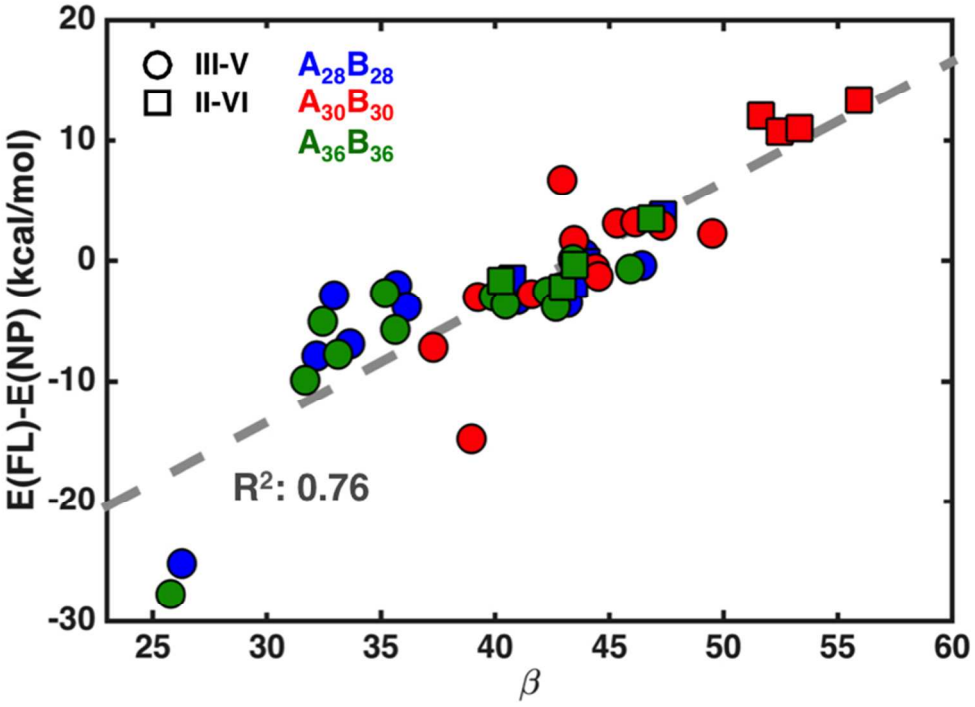

82x58mm (300 x 300 DPI)

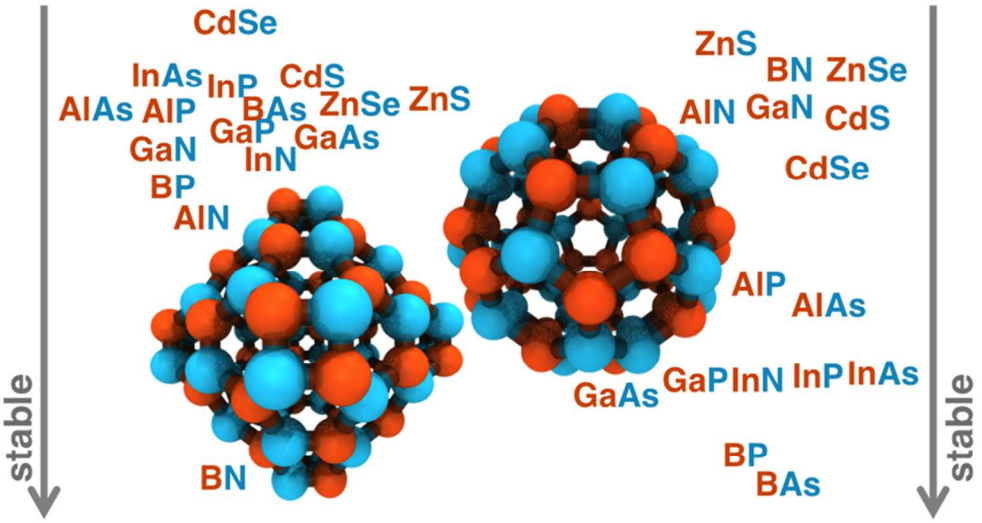

79x44mm (300 x 300 DPI)

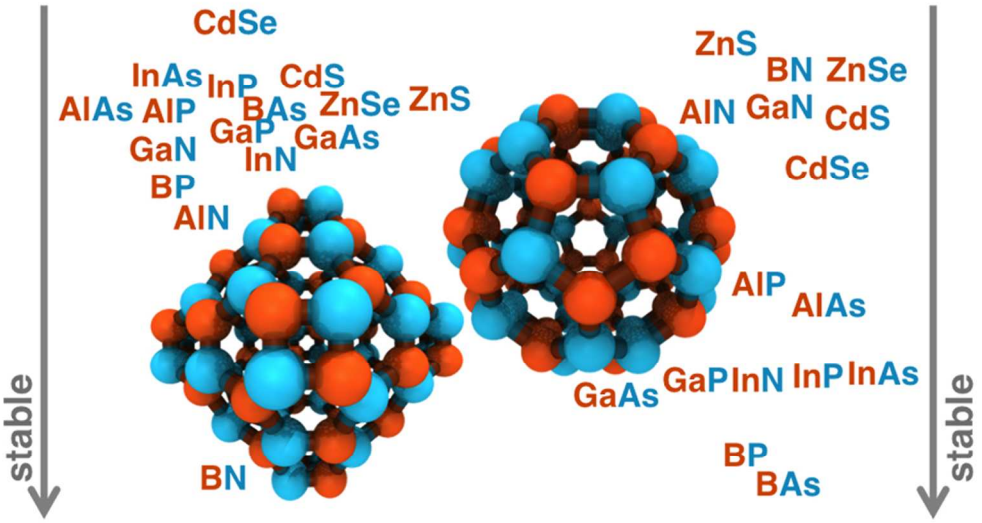

79x44mm (300 x 300 DPI)